Updated climatological mean delta fCO_2 and net sea–air CO_2 flux over the global open ocean regions

Amanda R. Fay[1], David R. Munro[2,3], Galen A. McKinley[1], Denis Pierrot[4], Stewart C. Sutherland[1], Colm Sweeney[3], Rik Wanninkhof[4]

Affiliations:
[1] Columbia University and Lamont-Doherty Earth Observatory, Palisades, NY, USA
[2] Cooperative Institute for Research in Environmental Sciences (CIRES), University of Colorado, Boulder, CO, USA
[3] Global Monitoring Laboratory, National Oceanic and Atmospheric Administration, Boulder, CO, USA
[4] Atlantic Oceanographic and Meteorological Laboratory, National Oceanic and Atmospheric Administration, 4301 Rickenbacker Causeway, Miami, FL, USA

Corresponding author: Amanda R. Fay afay@ldeo.columbia.edu

Key Points

- An updated surface water CO_2 climatology for 1980-2021 is created using the SOCAT database, following procedures of Takahashi et al. (2009)
- A net air-sea CO_2 flux of -1.79 ± 0.7 PgC yr-1 is determined for near-global ocean coverage

Abstract

The late Taro Takahashi (LDEO/Columbia University) and colleagues provided the first near-global monthly air-sea CO_2 flux climatology in Takahashi et al. (1997), based on available surface water partial pressure of CO_2 measurements. This product has been a benchmark for uptake of CO_2 in the ocean. Several versions have been provided since, with improvements in procedures and large increases in observations, culminating in the authoritative assessment in Takahashi et al. (2009). Here we provide and document the last iteration using a greatly increased dataset (SOCATv2022) and determining fluxes using air-sea partial pressure differences as a climatological reference for the period 1980-2021 (Fay et al. 2023). The resulting net flux for the open ocean region is estimated as -1.79 ± 0.7 PgC yr^{-1} which compares well with other global mean flux estimates. While global flux results are consistent, differences in regional means and seasonal amplitudes are discussed. Consistent with other studies, we find the largest differences in the data-sparse southeast Pacific and Southern Ocean.

Really short plain language statement:
Presented here is a near-global monthly estimate of the difference between atmosphere and ocean carbon dioxide concentrations. The ocean's ability to take up carbon, both now and in the future, is defined by this difference in concentrations. With over 30 million measurements of surface ocean carbon over the last 40 years, and utilization of an extrapolation technique, a mean estimate of surface ocean delta fCO2 is presented.

1. Introduction

As of the start of the 2020s, atmospheric carbon dioxide (CO_2) levels exceed 415 ppm on an annual basis and the continued growth of the atmospheric reservoir represents a major societal concern due to the impact on the radiative balance of the atmosphere. Warming and associated environmental changes including sea-level rise and ocean acidification have adverse effects on countless aspects of terrestrial and marine ecosystems which in turn impact air-sea exchange of CO_2 and the trajectory of the atmospheric CO_2 levels. The annually updated Global Carbon Budget (GCB) report estimates current net global ocean carbon uptake has been estimated at nearly 3.0 PgC per year, which corresponds to about a quarter of the total annual emissions (the total anthropogenic CO_2 emission, including the cement carbonation sink, is estimated at 10.9 ± 0.8 PgC yr^{-1}) (Friedlingstein et al. 2022). Given the importance of the ocean as a CO_2 sink, it is essential to continuously monitor changes and improve our understanding of the ocean's role in the global carbon cycle.

Deleted: Atmospheric

Deleted: now

Over the last several decades, multiple approaches based on atmospheric and oceanic observations have been developed to measure the impact of the ocean on the global CO_2 cycle. These approaches include atmospheric inversions (Feng et al. 2019), global atmospheric O_2/N_2 (Manning & Keeling 2006), ^{13}C measurements (Quay et al. 1992, Tans et al. 1993), ocean inventory approaches (Gruber et al. 2023) and the measurement of surface ocean and atmospheric CO_2 (Takahashi et al. 1993). All methods work towards the goal of elucidating the net flux of CO_2 from the atmosphere into the ocean. These different approaches have multiple advantages and disadvantages depending on the time and spatial scale of interest. Directly measuring surface ocean and atmospheric CO_2 levels has the advantage, given sufficient measurements, of deriving spatial and temporal variability over the ocean surface on short temporal and spatial scales. This method provides valuable insights into key processes driving the uptake and emissions of carbon when combined with our understanding of ocean physics and biological activity.

The surface ocean and atmospheric CO_2 approach leverages available observations and the dynamic sea-air gradient between the partial pressure of carbon dioxide (pCO_2) in the surface ocean (pCO_2^{oce}) and the overlying atmosphere (pCO_2^{atm}), known as the delta pCO_2 (ΔpCO_2) and typically defined as pCO_2^{oce} - pCO_2^{atm}. This difference is the thermodynamic driving force for the transfer of CO_2 into (negative) and out of (positive) the ocean. On average, the ΔpCO_2 across the global oceans are becoming increasingly negative as atmospheric CO_2 levels steadily rise, leading to an increasing carbon sink. Limited regions around the globe are sources of CO_2 to the atmosphere, including the equatorial Pacific Ocean and other areas of persistent upwelling.

The late Taro Takahashi was a leader in efforts to characterize air-sea CO_2 flux through the design and deployment of pCO_2 systems throughout the global oceans, and perhaps most importantly, his efforts to assemble, evaluate and construct global ocean climatologies from available pCO_2^{oce} datasets. Building on early collaborative work looking at ocean sources and sinks of carbon (Tans et al. 1990), many versions of the ocean pCO_2 climatology have been presented in literature (Takahashi et al. 1997, 2002, 2009a,b, and 2014), henceforth referred to as T-1997, T-2002, T-2009, and T-2014. The climatologies have been highly utilized and cited by carbon cycle researchers from around the world, and form a basis for current advancements in quantifying the ocean carbon sink.

Here, we present an updated near-global climatological mean distribution and net sea–air CO_2 flux which represent the mean of ocean conditions over the last four decades. This climatology is unique compared to other advanced machine learning approaches (e.g., Rödenbeck et al. 2015) in that it interpolates in time and space using only the

Deleted:); all

Deleted: These

Deleted: 2009

Deleted: ; all of which

Deleted: . We

available pCO_2 data rather than using proxy variables for gap filling. This difference in methodology provides a valuable alternative approach to the ongoing effort to characterize the global ocean carbon sink. This benchmark is critical for global carbon assessments, notably the Regional Carbon Cycle Assessment and Processes (RECCAP2, DeVries et al. 2023) effort.

Building on previous work of Takahashi and colleagues, we employ the same time-space interpolation method used in the previous versions of the Takahashi climatology (e.g., T-2002, T-2009, T-2014) to create the climatology. However, here we use the Surface Ocean CO_2 Atlas (SOCAT) v2022 database (Bakker et al. 2016, 2022), rather than the LDEO database curated by Taro Takahashi. We use the SOCAT database for this update because it is the most comprehensive database of available observations from international research groups. We have included the climatology produced using the most recent LDEO database (LDEOv2019, Takahashi et al. 2020) with data extending to 2019, in supplementary figures and text but our main findings will focus on the results from the SOCAT database.

2. Data

2.1 SOCAT database

The SOCAT database was first released in 2011 (Pfeil et al. 2013) and is updated annually (Bakker et al. 2016). Observations are reported as values of fugacity of CO_2 (fCO_2) in micro atmospheres (µatm), along with a collection of ancillary data including concurrent observations such as SST (more accurately, the ship intake temperature), temperature of equilibration, salinity, and sea level pressure at the time of equilibration. The SOCAT database also includes supplemental variables with values interpolated from gridded global datasets such as satellite SST and NCEP sea level pressure. The database restricts the included data to only observations that are measured in near-continuous operation or in discrete samples with an equilibrator system. This means that it does not include fCO_2 values that are calculated from other ocean carbon measurements including dissolved inorganic carbon, total alkalinity and/or pH. For this analysis we select SOCAT data from cruises with flags A-D and observations with a World Ocean Circulation Experiment (WOCE) flag of 2 (Pfeil et al. 2013). More information on the SOCAT database is available in Bakker et al. (2016); current and previous releases are available to download at https://www.socat.info/index.php/data-access/.

Deleted: 2013

Deleted: ; specifically,

The SOCAT database (Bakker et al. 2016) is the largest and most widely used collection of quality-controlled fCO_2 data with over twice the number of observations included in the latest LDEO database (LDEOv2019). In this work, we utilize the SOCATv2022 release which includes over 33.7 million observations spanning the years 1957 through 2021 (DOI:10.25921/1h9f-nb73, accessed on July 15, 2022, Bakker et al., 2022). We use observations beginning in 1980 due to limited metadata available for earlier observations. This time restriction eliminates only 24,786 observations, or less than 0.1% of the total number of observations included in the SOCATv2022 release. We also exclude coastal observations collected within 100km of land similar to past LDEO climatologies which reduces the total number observations utilized to just over 21.3 million. Unlike past LDEO climatologies, this climatology does not exclude observations collected in the equatorial Pacific during El Niño periods.

2.2 fCO_2 vs pCO_2

For this climatology, we report values of the fugacity of carbon dioxide (fCO_2) rather than pCO_2. The fCO_2 is equal to the pCO_2 corrected for non-ideality of CO_2 solubility in water using the virial equation of state (Weiss 1974). The fugacity correction for surface water is 0.996 and 0.997 at 0 ºC and 30 ºC respectively (Dickson et al. 2007), or 0.7 to 1.2 µatm lower than the corresponding pCO_2, and depends primarily on temperature for the conversion although pressure is also included in the conversion equation. It is now common practice in the observational community to present observed values as fCO_2 and this option has been endorsed by the IOCCP (International Ocean Carbon Coordination Project). The correction of pCO_2^{oce} and corresponding pCO_2^{atm} values to fCO_2 is practically identical such that the resulting ΔfCO_2 is always within 0.1 µatm compared to the corresponding ΔpCO_2. As a result, this difference will not have a meaningful impact on air-sea flux calculations. Only at elevated fCO_2 levels, such as those in the subsurface ocean, is the difference between fCO_2 and pCO_2 significant. Therefore, the shift in this climatology from pCO_2 to fCO_2 simply aligns this updated climatology with current community best practices. This choice avoids conversions given that the SOCAT database reports fCO_2 values.

2.3 Distribution of measurements

At present, the SOCAT database relies on voluntary submission of quality-controlled data from over 100 scientists. The number of observations has increased significantly over past decades, facilitated by a now-automated data submission process. Even with this increase in observations, there are only a few regions over the global oceans where fCO_2^{oce} has been systematically monitored over multiple decades at nearly the same location (Bakker et al. 2016; Bates et al. 2014; Landschützer et al. 2016, Figure 1). Of

Deleted:

the observations considered in this analysis, spanning years 1980-2021, only 1.4% of the monthly 1º by 1º global ocean grid cells have measured values. Most of the data (65%) was collected since 2010.

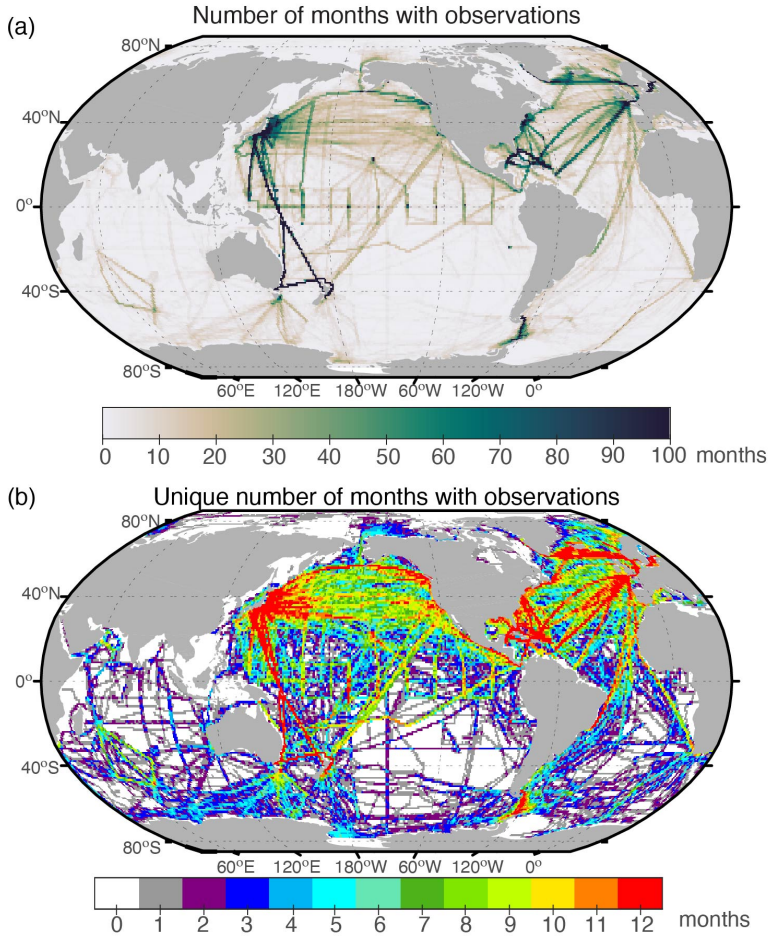

Figure 1: (a) Total number of months with at least one observation in each 1º grid cell in the SOCATv2022 database, for years 1980-2021 (Bakker et al. 2022). The maximum number possible for a grid cell is 504 (42 years * 12 months). (b) the number of unique calendar months in each grid cell where at least one observation has been made since 1980. Red indicates grid cells where each month (Jan - Dec) has been sampled at least once over the 40+ year time series while white indicates grid cells with no measurements over the length of the time series.

An additional challenge to global monitoring efforts is that observations are not collected consistently throughout the annual cycle in many locations around the globe, thus requiring considerable interpolation to produce a full seasonal climatology. Much of the ocean contains data collected in fewer than three unique months of the year, regardless of how many years of data is available (Figure 1b). Current efforts utilize proxy variables and machine learning to identify relationships between ocean carbon and better-observed variables (often SST, chlorophyll, mixed layer depth, etc.) and then through those relationships extrapolate available ocean fCO_2 to fill the missing months of the seasonal cycle. Unlike those methods (e.g., methods compared by Rödenbeck et al. 2015), we do not utilize any proxy variables in this method and only rely on available fCO_2^{oce} values in the SOCAT database to estimate the seasonal climatology. Hence, this effort provides a complementary alternative interpolation method to other approaches.

2.4 Atmospheric fCO_2

For the calculation of atmospheric carbon dioxide, we utilize zonally invariant NOAA marine boundary layer (MBL) xCO_2 values which are reported in units of ppm or µmol/mol (Lan et al. 2023) and provided with each observation in the SOCAT dataset. In order to calculate fCO_2^{atm} values from MBL xCO_2^{atm} values, we follow standard operating procedures and equations outlined in Dickson et al. (2007) and use the SST, salinity and sea level pressure observations also reported for each value in the SOCAT database (Bakker et al. 2022). The SST (more specifically, ship intake temperature) is measured concurrently with surface ocean CO_2, sea level pressure is from the National Centers for Environmental Prediction (NCEP), and surface salinity is from the World Ocean Atlas (WOA). Delta fCO_2 (ΔfCO_2) is calculated by subtracting corresponding atmospheric from ocean values (fCO_2^{oce} - fCO_2^{atm}).

3. Methods

3.1 Normalization to a reference year

In previous versions of the LDEO climatology, emphasis was placed on the calculation of trends in surface ocean carbon levels for all regions of the global ocean. These trends were used to normalize all available observations to one reference year by correcting for the estimated change that would be expected between the collection date of the observation and the reference year. In this updated climatology, we use ΔfCO_2 values as input to the algorithm rather than allowing for the adjustment of fCO_2^{oce} to a specific reference year. A similar methodology was used in early versions of the LDEO climatology (i.e., T-1997).

By utilizing this method to collapse all available data to one year, we make the assumption (as made by T-1997) that the ocean and atmosphere are changing at the same rate and thus the ΔfCO_2 has been constant over the 40+ years of observations. This assumption allows for a standard method for the normalization of all observations to one calendar year. This method is utilized in contrast to the most recent LDEO climatologies where trends over distinct time periods were investigated and one trend then selected for use in time-normalization throughout much of the global ocean (i.e., T-2002, T-2009, and T-2014).

Atmospheric pCO_2 change drives rising ocean pCO_2, and surface ocean carbon concentrations follow atmospheric increases on multi-decadal timescales and over large regions and the global scale (Fay & McKinley 2013, McKinley et al. 2020). Large synthesis efforts by those in the global ocean carbon community show that even if ocean trends are larger/smaller than the atmosphere on decadal or multi-year time periods, when considering the longest time periods, the atmosphere and ocean carbon trends are statistically indistinguishable over much of the global ocean (Fay & McKinley 2013, Tjiputra et al. 2014). While the Tjiputra et al (2014) and Fay & McKinley (2013) efforts consider large regional analysis, Bates et al. (2014) provides a synthesis of trends in pCO_2 at long-term observing stations, with most of the stations showing a match to the rise in atmospheric CO_2 concentration (Tanhua et al. 2015).

Supplementary Table 1 shows biome-scale mean fCO_2 trends computed using all available 1ºx1º grid cells with observations in the gridded product released as part of SOCATv2022 (Sabine et al. 2013). We present seasonal trends for each biome due to seasonal sampling bias over much of the global oceans. Similar to T-2009 (see Tables 1-5 of T-2009), trends for different ocean regions vary significantly (Supplementary Table 1) due in part to differing years with available data across ocean regions

(Supplementary Figure 5). Observations within the Indian Ocean, for example, and other regions with blue shading in Supplementary Figure 5 are weighted towards the 1980's and 1990's while regions stretching across the North Atlantic and North Pacific have been heavily sampled over the last two decades with ships of opportunity. These well sampled regions have median years of collected observations later than 2010 (areas with red shading in Supplementary Figure 5).

Recent studies (Friedlingstein et al. 2022) demonstrate that globally, the oceans lag slightly behind the atmosphere in terms of rates of carbon increase, and thus ΔfCO_2 has become increasingly negative as noted above. The central climatological year represented by our method is thus somewhat ambiguous regionally, though globally it is centered at about 2010. The median year of all fCO_2 observations collected in SOCATv2022 greater than 100km from land is 2013. Since observations are more densely clustered in the recent period, observations in the early period may have a greater weight in determining climatological values. Given global trends, our approach may estimate a smaller ocean sink in regions where the ocean was sampled more heavily early in the time period (e.g., blue shading in Supplementary Figure 5) and a greater ocean sink in regions with heavy recent sampling (red shading in Supplementary Figure 5). We acknowledge that the assumption of a constant ΔfCO_2 does not take into account the long-term trend in ΔfCO_2, however, our simplified approach avoids application of trends determined for well-observed regions and time periods across poorly-observed regions and time periods.

We conducted a sensitivity analysis to demonstrate the impact of the ΔfCO_2 method implemented in this version versus a normalization approach similar to that applied in T-2009. Specifically, we assumed a homogeneous 1.5 µatm yr^{-1} trend in fCO_2^{oce} for all regions and years, and normalized available observations to a reference year of 2010. Spatial maps of the differences in fCO_2 for the year 2010 for the normalization approach versus ΔfCO_2 method are shown in the supplemental information (Supplementary Figure 6). Globally, the annual ocean uptake created using the 1.5 µatm yr^{-1} normalization method (T-2009) is within 3% of the ΔfCO_2 method (this analysis)- specifically, -1.85 PgC yr^{-1} versus -1.79 PgC yr^{-1} for the 1.5 µatm yr^{-1} normalization method and the presented ΔfCO_2 approach, respectively, for a reference year of 2010.

3.2 Method for time–space interpolation

The method for spatial interpolation and day of year utilized in the climatology has not changed from the previous versions (e.g., T-2009). As described above, ΔfCO_2 values are used to compile observations into one reference year in contrast to the time-normalization approach of T-2009. The spatial interpolation scheme requires that all

Deleted: ;

Deleted: ; the

Deleted: ; since

Deleted:);

observations are binned into 4ºx5º grids for each day of the year. In some areas of the global ocean, such as the northern and equatorial ocean regions, there are observations in a majority of the pixels. However, vast expanses in the Southern Hemisphere have few observations in each pixel and there are many pixels that contain no observations at all (Figure 1).

We follow the same methodology as T-2009 for binning observations in sparsely sampled grid cells south of 12ºS. Here, spatial binning is increased by 4º and 5º longitude and latitude, respectively, extending from the center of each grid cell. This creates a grid of overlapping 8ºx10º grid cells. Additionally, bins include the day before and after a given day of year. The mean is computed by weighting measured values inversely proportional to their time-space distance from the pixel center. After the above procedures are applied, more than 50% of the space–time pixels over the global oceans are filled.

To estimate the ΔfCO_2 values in the remaining cells, an interpolation equation based on the 2-D diffusion–advection transport of surface waters is used, as in T-2009. The equation is discretized onto a 4ºx5º grid for the global ocean, and solved iteratively using a finite difference algorithm (Takahashi et al. 1995, T-1997). The method avoids singularities at the poles by assigning land to each high latitude region (Antarctica in the south and treating the highest latitudes of the Arctic Ocean as land in the north). With this method, the resulting ΔfCO_2 values are the solutions obtained after 500 iterations, as previously determined on the basis of interpolation experiments of temperature values (T-2009).

With this interpolation scheme, observed ΔfCO_2 values where available are preserved, and the continuity equation is used to compute values for grid cells that have no observations. Consistent with previous iterations of this approach, the combined effects of internal sources and sinks of carbon, CO_2 exchange with the atmosphere, as well as upwelling of deep waters are all assumed to be included in the analysis of the observations that feed into the interpolation scheme. Uncertainties persist due to the sparsity of input data, normalization to a reference year, and the space-time interpolation. In part to address these uncertainties, we report only monthly means.

To maintain consistency with similar products and input datasets for flux calculations, we downscale to one-degree boxes by assigning all 20 1ºx1º pixels in a 4ºx5º grid cell the same ΔfCO_2 value. When calculating sea-air fluxes, because the other inputs to the flux calculation such as wind speed, are varying on a 1ºx1º degree resolution grid, differences in the gridded flux climatology emerge on this finer spatial scale.

Deleted:

3.3 Flux calculation method: pySeaFlux

To assess the near-global ocean carbon sink associated with these ΔfCO_2 estimates, air-sea CO_2 exchange must be calculated. The gridded monthly 1ºx1º ΔfCO_2 values were used to compute air-sea CO_2 fluxes using the bulk formulation with python package Seaflux.1.3.1 (https://github.com/lukegre/SeaFlux, Gregor & Fay, 2021). The net sea–air CO_2 flux (F) is estimated using:

$$Flux = kw \cdot sol \cdot (fCO_2^{oce} - fCO_2^{atm}) \cdot (1 - ice) \quad \text{Eq. (1)}$$

where kw is the gas transfer velocity, sol is the solubility of CO_2 in seawater (in units of mol m^{-3} μatm^{-1}), fCO_2^{oce} is the partial pressure carbon in the surface ocean (in µatm), and fCO_2^{atm} (in units of µatm) represents the atmospheric CO_2 levels in the marine boundary layer. Finally, to account for the seasonal ice cover at high latitudes, the fluxes are weighted by one minus the ice fraction (ice), i.e., the open ocean fraction. By utilizing the pySeaFlux package (Fay & Gregor et al. 2021, Gregor & Fay 2021), we are able to include multiple scaled gas transfer velocities for three different wind products and our resulting flux estimate is a mean of the three. Additional inputs to the flux calculation include EN4.2.2 salinity (Good et al. 2013), SST and ice fraction from NOAA Optimum Interpolation Sea Surface Temperature V2 (OISSTv2, Reynolds et al., 2002), European Centre for Medium-Range Weather Forecasts (ECMWF) ERA5 sea level pressure (Hersbach et al. 2020). Finally, surface winds and associated wind scaling factor for the Cross-Calibrated Multi-Platform v2 (CCMP2; Atlas et al. 2011), the Japanese 55-year Reanalysis (JRA- 55; Kobayashi et al. 2015), and the ECMWF ERA5 (Hersbach et al. 2020) reanalysis products are used.

Fluxes reported here use inputs from the year 2010 for the kw, sol, and ice fraction variables. Alternatively, we have calculated fluxes using a mean over a 17-year time period centered on the year 2010. This yields a very similar value with the mean difference being a 0.04 PgC yr^{-1} increase in estimated carbon uptake.

4. Results

4.1 Climatological mean distribution of surface water ΔfCO_2

4.1.1 Global

The near-global 12-month climatological mean distribution of ΔfCO_2 (fCO_2^{oce} minus fCO_2^{air}) is reported for the SOCAT database (Figure 2, Fay et al. 2023). Evident in the mapped climatology are the large-scale patterns across the global ocean: the consistent

high (positive) ΔfCO_2 values in the equatorial Pacific region where upwelling is a dominant influence, and low (negative) values of ΔfCO_2 in the North Atlantic region where evaporation leads to increase salinity and cooling driving strong uptake of carbon and subduction of surface waters.

A near-global mean climatology curve shows a bimodal shape in ΔfCO_2, with a smaller peak in boreal spring (March/April) and a much larger peak in late boreal summer (August/September), clearly driven by the hemispheric seasonal cycles (Figure 2a). The global curve reaches its minimum in November and begins a recovery throughout the boreal winter before dipping again to a springtime minimum in June. The near-global annual mean ΔfCO_2 value is -4.1µatm (with temporal standard deviation equal to 1.6 µatm) and it is notable that the global mean ΔfCO_2 value is below zero for every month of the year, suggesting that seasonally the global ocean mean is a perpetual carbon sink with expansive regions of uptake nearly always outweighing smaller regions of efflux (Figure 2, 3). On the other hand, the northern and southern hemispheric seasonal cycles each exhibit peaks in ΔfCO_2 above zero during their corresponding warm/summer months (Figure 2a).

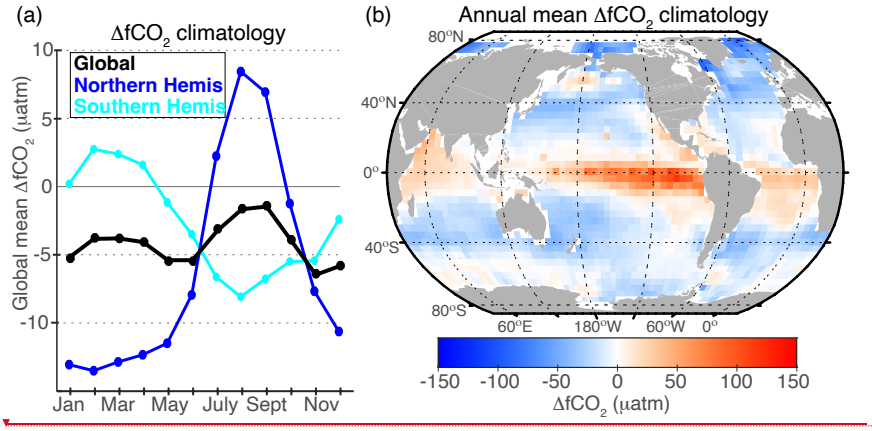

Figure 2: (a) Global mean and Northern and Southern Hemisphere ΔfCO_2 seasonal climatology from the SOCAT database, (b) Map of annual ΔfCO_2 climatology.

Deleted:). The

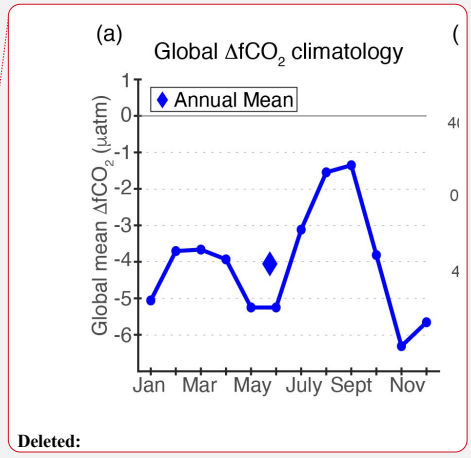

Deleted:

Deleted: ; annual mean value is indicated by the diamond (-4.1µatm).

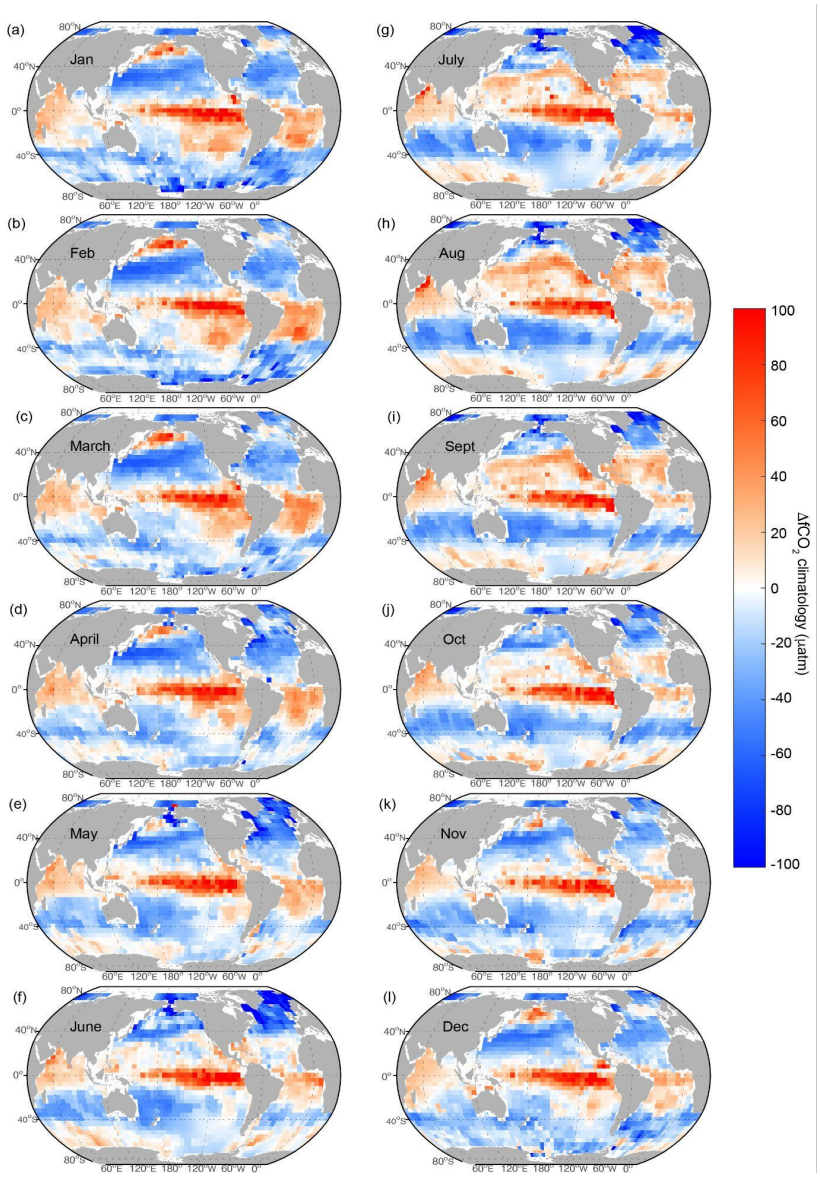

Figure 3: Monthly mean values for sea–air ΔfCO_2. Warm colors indicate positive ΔfCO_2 (ocean is greater than atmospheric CO_2), white indicates near zero ΔfCO_2, and cool colors indicate negative ΔfCO_2 (ocean CO_2 is lower than the atmosphere).

4.1.2 Regional

To show the seasonal changes in ΔfCO_2 more clearly it is valuable to consider the patterns exhibited over consistent biogeochemical regions around the globe. For this analysis we utilize the biomes of Fay & McKinley (2014), but for simplicity we combine the seasonally stratified and permanently stratified subtropical biomes into one region in the Northern Hemisphere (referred to simply as subtropical in this manuscript). Monthly climatologies for each of the biomes are shown (Figure 4) in addition to the gridscale maps for each climatological month which allows for further regional interpretation (Figure 3). Table 1 lists the annual mean ΔfCO_2 values in each of these regions.

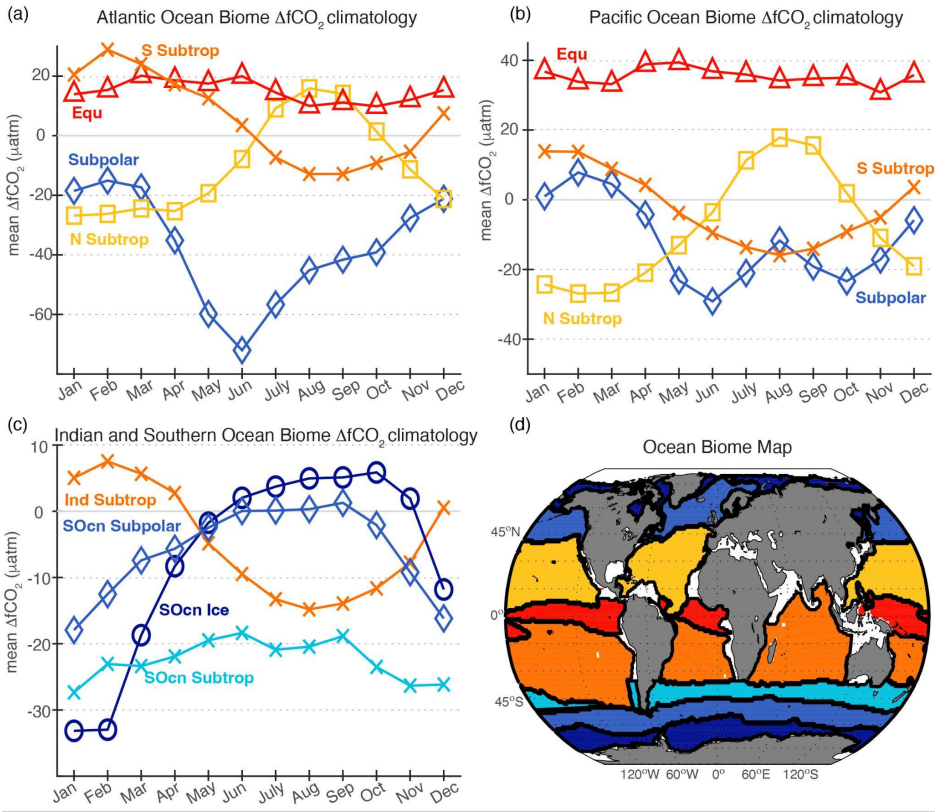

Figure 4: Monthly climatology of ΔfCO_2 for each regional ocean biome in the (a) Atlantic, (b) Pacific, (c) Indian and Southern Ocean basins. (d) Map of regional biomes. Colors of curves correspond to regions on the map in (d) with labels in matching colored text.

Note that the y-axis varies between subplots. Values for each region's annual mean and standard deviations listed in Table 1.

The equatorial regions of the Pacific and Atlantic oceans have positive ΔfCO_2 values throughout the annual cycle and little seasonal variability. This indicates that the area is a source of CO_2 to the atmosphere year round. The equatorial Pacific (Figure 4b) has the highest positive ΔfCO_2 values (annual mean = 35.4 µatm), followed by the tropical Atlantic (Figure 4a, annual mean = 14.8 µatm).

The subtropical biomes, representing the temperate North and South Atlantic and Pacific basins exhibit large seasonal ΔfCO_2 cycles which change sign throughout the year. Here, the ΔfCO_2 cycle is largely temperature driven, Positive ΔfCO_2 in warm summer months and negative values in colder winter months reflecting the dominance of seasonal temperature changes on the cycles of ocean fCO_2 in these regions. The seasonal amplitude for the subtropical North Pacific is 44.7 µatm, and is slightly larger than the seasonal amplitude in the subtropical North Atlantic (42.7 µatm). Since the mean seasonal amplitudes for SST are quite similar in these two ocean basins, with the Atlantic having a slightly larger seasonal change in surface temperature (4.4ºC in Pacific and 5.0ºC in Atlantic, not shown), the difference in ΔfCO_2 amplitudes between the Pacific and Atlantic subtropical regions cannot be attributed solely to SST, and may reflect differences in biogeochemical cycling between these two basins.

Deleted: ; positive

Seasonal changes in the northern subtropical oceans are roughly six months out of phase from the southern subtropical biomes. The South Pacific subtropical biome has a seasonal amplitude of 29.8 µatm which is nearly 15 µatm smaller than that of the North Pacific subtropical biome. In contrast, the seasonal amplitude of the South Atlantic subtropical basin is just 1 µatm smaller than its counterpart in the North Atlantic (the South Atlantic subtropical amplitude is 41.7 µatm). The Indian Ocean subtropical biome which encompasses most of the Indian Ocean, both above and below the Equator, has a smaller ΔfCO_2 amplitude (22.3 µatm), but the phasing matches well with both the South Pacific and South Atlantic subtropical biomes, with peak (positive) ΔfCO_2 values in February and the lowest values in August. The smaller ΔfCO_2 seasonal amplitudes in the Indian and South Pacific subtropical basins are partially attributable to lower SST variability in these regions (SST seasonal cycle amplitudes are 4.0ºC and 3.0ºC in the South Pacific and Indian subtropics, respectively, compared to 4.6ºC in the subtropical South Atlantic). However, it is likely that both differences in spatiotemporal patterns of primary productivity and undersampling in the South Pacific and Indian subtropics (Figure 1) also contribute to differences in ΔfCO_2 seasonal amplitudes between these basins.

The timing of the ΔfCO_2 trough in the subpolar regions is opposite that of the subtropical North Pacific and Atlantic basins. Strongly negative ΔfCO_2 in the spring and summer months is due to the effects of intense biological drawdown which quickly and dramatically lowers carbon levels in the subpolar surface ocean with the onset of the growing season. Biological productivity and strong spring/summer stratification result in subpolar seasonal cycles that are roughly four to six months out of phase compared to adjacent subtropical regions. In the Atlantic subpolar biome, ΔfCO_2 values are consistently below zero throughout the annual cycle (a maximum of -15.1 µatm occurs in February). In the subpolar North Pacific basin, positive ΔfCO_2 values are present over the boreal winter (Jan-March) before biological drawdown associated with the spring bloom lowers the ΔfCO_2 values back below zero for the remainder of the year. The spring drawdown is weaker in the subpolar North Pacific compared to the subpolar North Atlantic.

Figure 4c displays the seasonal cycle for the Southern Ocean biomes including the seasonal ice biome, the subpolar region, and the seasonally stratified subtropical region of the Southern Hemisphere. The higher latitude subtropical region has negative ΔfCO_2 values throughout the year and a relatively small seasonal ΔfCO_2 amplitude compared to the more expansive South Atlantic, South Pacific and Indian subtropical basins to the north. The mean ΔfCO_2 and seasonal amplitude for the Southern Ocean subtropical region is -22.5 µatm and 9.0 µatm, respectively.

The Southern Ocean subpolar and ice biomes both have relatively strong seasonal cycles, reaching maximums of ΔfCO_2 near and slightly above zero, respectively, during the late austral winter and early austral spring (Figure 4c). This positive peak during July through October in the Southern Ocean seasonal ice zone is influenced by under-ice vertical mixing with deep waters that contain excess carbon and nutrients. During the austral spring and summer months, intense phytoplankton blooms occur near and around the edges of the retreating sea ice in the seasonal ice zone and within the subpolar region. These blooms cause dramatic drops in ΔfCO_2 values at the end of the calendar year (Oct-Dec). Limited sampling and smoothing from the interpolation method fail to capture the high spatiotemporal variability that characterizes this highly dynamic region.

Biome	ΔfCO2 (µatm)	Flux (PgC yr^{-1})	Area (10^6 km^2)
NP Ice	-24.6 (9)	-0.02 (0.02)	4.2
NP SPSS	-11.5 (12)	-0.11 (0.11)	12.8

NP Subtropics	-8.2 (16)	-0.40 (0.53)	47.9
Pacific Equ	35 (2)	0.35 (0.03)	26.4
SP Subtropics	-2.3 (10)	-0.14 (0.31)	52.7
NA Ice	-19.3 (4)	-0.04 (0.01)	4.5
NA SPSS	-36.2 (17)	-0.27 (0.08)	9.7
NA Subtropics	-10.0 (16)	-0.24 (0.26)	23.4
Atlantic Equ	14.7 (3)	0.04 (0.01)	7.4
SA Subtropics	5.6 (14)	0.01 (0.12)	18.1
Indian Subtropics	-4.5 (8)	-0.18 (0.16)	35.9
SO STSS	-22.1 (3)	-0.59 (0.06)	29.6
SO SPSS	-6.0 (6)	-0.21 (0.22)	30.7
SO Ice	-6.8 (14)	-0.08 (0.12)	18.7

Table 1. Mean annual DfCO2 and flux in global open ocean biomes (Fay & McKinley 2014). Value in parentheses is one standard deviation over the 12-month climatology. Area of each biome also included. NP: North Pacific; SP: South Pacific; NA: North Atlantic; SA: South Atlantic; SO: Southern Ocean. SPSS: Subpolar seasonally stratified; STSS: Subtropical seasonally stratified. Northern hemisphere subtropical regions are reported to match the regions shown in Figure X (combining the STPS and STSS biomes from Fay & McKinley 2014 into one).

4.2 Net air-sea CO_2 flux

The mean climatological global air-sea CO_2 flux estimate using the SOCAT database is -1.79 PgC yr^{-1}, indicating uptake of carbon by the ocean. This is a slightly greater flux into the ocean than the direct estimate from the previous version of the climatology (T-2009), which reported a direct estimated global mean flux of -1.4 PgC yr^{-1} for the year 2000. For the uncertainty in global ocean-atmosphere CO_2 flux, we use the methods described in T-2009 with updated uncertainty estimates as reported when applicable. Wanninkhof et al. (2013) followed the same approach as T-2009 with consideration of updated synthesis work (Ho et al. 2011). Our approach combines uncertainty contributions from the spatial (13% or ±0.23 (T-2009)) and temporal (±0.5 PgC yr^{-1} (T-2009)) sampling of ΔfCO_2 as well as smaller contributions for the uncertainty in the gas exchange parameterization (20% or ±0.36 PgC yr^{-1}, Wanninkhof 2014), wind (±0.09 PgC yr^{-1} (Fay & Gregor et al. 2021) and riverine carbon (±0.2 PgC yr^{-1}, Jacobson et al., 2007). This yields an uncertainty estimate of ±0.7 PgC yr^{-1} (when summed in quadrature) on our mean climatological global air-sea CO_2 flux estimate.

Deleted: value reported by

Deleted: who

Deleted: . This

Deleted: (±0.18 and ±0.5 PgC yr^{-1}, respectively)

Deleted: (±

Deleted: 2

Deleted: 15

Deleted:).

Results discussing the net flux produced from the LDEO pCO_2 database climatology is included in the supplementary material.

4.2.1 Mean annual distribution

The near-global mean flux estimate presented here represents 90% of the surface area of the global ocean. Specifically, this estimate excludes the coastal ocean and areas of the high latitude seas. We have chosen to present the near-global flux value discussed above without any adjustment to which could account for missing areas. Suggested methods for filling missing ocean areas in such reconstructions are available in Fay & Gregor et al. (2021) but are not implemented in this climatology to remain consistent with its previous versions. An estimate of the flux from regions missing from this product can be obtained by using the full-coverage pCO_2 climatology combining open and coastal oceans (Landschützer et al. 2020). Considering only grid cells in the Landschützer et al. (2020) product that are missing in this climatology, we estimate an annual average coastal and high latitude flux of -0.38 PgC yr^{-1}. The flux adjustment for missing areas of this climatology varies throughout the seasonal cycle, ranging from -0.43 to -0.31 PgC yr^{-1} during the 12 months of the climatology. This quantity is not included in the climatological estimate presented here.

Deleted: values

Deleted: and acknowledge that this analysis represents a near-global estimate

Deleted:

Deleted: through

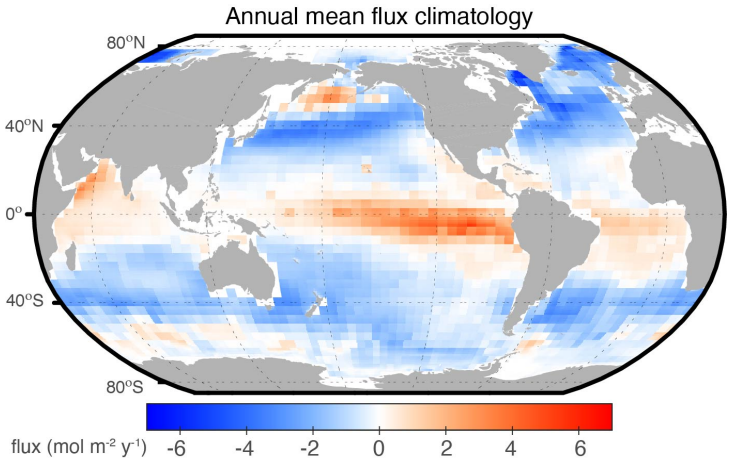

Figure 5: Annual mean CO_2 flux calculated from the SOCAT database. Flux is calculated using the SeaFlux method using the mean of three wind speed reanalysis products. Warm and cool colors indicate regions of carbon efflux and uptake, respectively. The near-global mean flux is -1.79 PgC yr^{-1}.

Figure 5 shows the climatological mean annual sea–air CO_2 flux (mol m^{-2} yr^{-1}) and maps of two seasons (DJF and JJA) are displayed in Figure 6. Annual mean sea-air CO_2 flux values for the ocean regions are summarized in Table 1. The equatorial Pacific is the most prominent atmospheric CO_2 source region, with a seasonally persistent sea-to-air flux of 0.35 PgC yr^{-1}. When combined with the equatorial Atlantic region, the tropical belt emits an annual mean of 0.39 PgC yr^{-1} to the atmosphere. Adjacent to this tropical efflux zone, are vast expanses of seasonally-variable flux patterns. The subtropical basins in both hemispheres act as CO_2 sinks in the cooler months and transition to regions of neutral or small CO_2 sources during the warmer months. At higher subtropical latitudes, strong winds and relatively low ocean fCO_2 occur along the subtropical convergence zone where the cooled subtropical gyre waters with low fCO_2 meet the subpolar waters with biologically-lowered fCO_2.

The Northern Hemisphere mid and high latitude regions represent a smaller sink compared to the corresponding regions of the Southern Hemisphere (Table 1) largely due to the overall greater surface area of the oceans in the Southern Hemisphere (oceans south of 35S are 25% of total global ocean area while oceans north of 35N are 15% of total ocean area). The dramatic influence of the expansive Southern Hemisphere oceans is also demonstrated by the large flux in the Southern Ocean subtropical region (-0.59 PgC yr^{-1}) that represents 8% of the global ocean surface area.

Deleted: (-0.63 PgC yr^{-1})

Deleted: (-0.91 PgC yr^{-1}

Moving poleward, a strong sink (-0.27 PgC yr^{-1}) occurs in the North Atlantic subpolar region which includes the Nordic Seas and the portions of the Arctic Ocean which contain observations. This strong localized carbon sink is attributed to the import of low anthropogenic waters at depth in the Gulf Stream that are exposed as mixed layers deepen (Ridge & McKinley 2020), and large phytoplankton blooms in spring followed by cooling in winter. In the Southern Ocean, annual mean CO_2 flux is heterogeneous and relatively small in the seasonal ice zone due to the ice cover that reduces sea–air gas transfer in winter. Additionally, the small annual flux values in the Southern Ocean subpolar and ice regions (-0.21 PgC yr^{-1} and -0.08 PgC yr^{-1}, respectively) are a result of a cancellation of the seasonal source (winter) and sink (summer) fluxes.

4.2.2 Seasonal variation of sea–air CO_2 flux

Seasonal variation in air-sea fluxes is clearly seen in the climatology (Figure 6) and are attributed to a combination of effects including fluctuations in SSTs, biological uptake of carbon dioxide, as well as mixing and wind speeds.

The seasonal variability of fluxes in higher latitudes of the subtropics in the Atlantic, Indian and Pacific Oceans cause an oscillation from neutral or weak sources of CO_2 to the atmosphere in the warmer seasons to strong CO_2 sinks in the cooler or winter seasons. Water cools as it is transported poleward by western boundary currents, allowing for carbon uptake (Ayers & Lozier 2012). In spring and summer, the biological drawdown of carbon increases CO_2 uptake by the ocean, partially offset by increases in fCO_2 due to warming.

Subtropical gyre regions also transition from weak sinks in the winter seasons to weak sources in the summer seasons, following the seasonal SST cycles and reflecting the dominance of temperature effects in controlling the seasonal variability in the fCO_2 and sea–air fluxes in oligotrophic gyres. In tropical low latitude regions, seasonality is generally smaller, however localized hot spots of high variability and large fluxes do exist, such as in the northwestern Indian Ocean where the strong summer monsoon winds force upwelling of carbon rich subsurface waters and cause high gas transfer rates in this region (Chen and Tsunogai 1998, T-2002, Sabine et al. 2000). The equatorial Pacific and Atlantic show little seasonal variability in CO_2 flux with a persistent efflux throughout the year.

Deleted: et al.

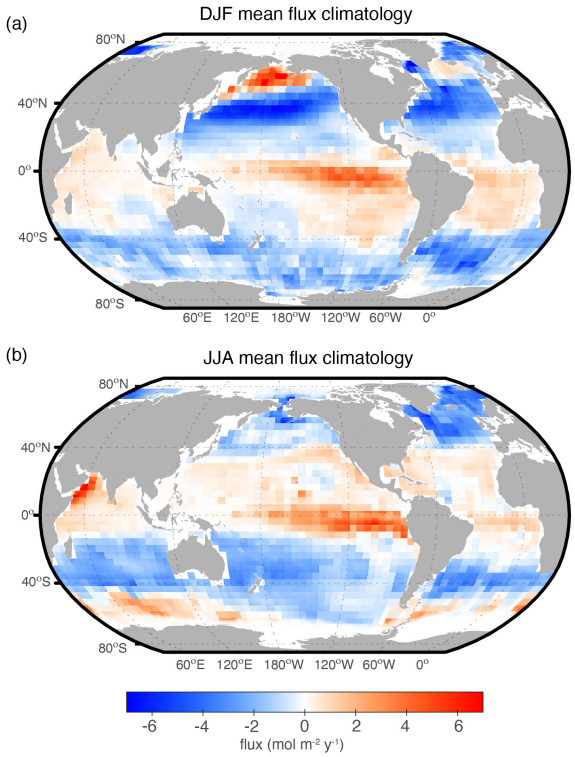

Figure 6: Season sea–air CO_2 flux (molC m^{-2} $year^{-1}$) climatology for (a) December, January, February (DJF) and (b) June, July, August (JJA). Positive values (warm colors) indicate sea-to-air fluxes (ocean efflux), and negative values (cool colors) indicate air-to-sea fluxes (ocean uptake).

In the Southern Ocean, there is a consistent region of moderate carbon source waters located in the Atlantic and Indian sector south of 45S latitude during the austral winter (Figure 6b). The source in the Southern Ocean region could be influenced by high fCO_2 waters from margins of the Antarctic sea-ice field given that the efflux values occur during the austral winter months (JJA). As the seasons transition to warmer temperatures and the ice edge recedes, this region is impacted by high rates of photosynthesis causing fCO_2 drawdown, and resulting in a transition to moderate carbon sinks during the austral summer (DJF). Another possibility is that the austral winter carbon source is linked to deep mixing and/or upwelling water which would bring an import of high DIC to the surface layers. Given the limited number of observations,

Deleted: Uncertainties are higher in the Southern Ocean region due…

particularly in winter in the Southern Ocean (Figure 1), confidence in the resulting climatology is lower in this region.

5. Discussion

It should be noted that there isn't one specific reference year for this release of the ΔfCO_2 climatology as was the case for previous releases (e.g., the year 2000 reference in T-2009). Instead, this climatology represents a multidecadal time period, beginning in 1980, with the majority of observations feeding into the climatology collected after 2010. Therefore, while the ΔfCO_2 climatology is not reported for a specific reference year, it is most representative of the conditions over the past two decades. We note however that the flux estimates given in this analysis are based on inputs from a single year, the year 2010, as described above in Section 3.3 (comparison of flux estimates using 2010 inputs and averages over several decades yield very similar results, also as described in Section 3.3).

5.1 Comparison with T-2009 climatology

In the previous release of this climatology (T-2009), pCO_2 values were corrected to a reference year of 2000 using a mean atmospheric CO_2 increase rate of 1.5 µatm yr^{-1} over the entire ocean area with the exception of the Bering Sea, where the observed rate of -1.2 µatm yr^{-1} was used. In our updated method described above (Section 3.1), we eliminate the need to apply a normalization rate for observations and instead calculate a ΔfCO_2 value for each observation using a co-located concurrent atmospheric fCO_2 value. We note that T-2014 presents a more updated pCO_2 climatology than T-2009. Since T-2014 emphasizes climatologies for the other carbonate system variables (pH, dissolved inorganic carbon, and total alkalinity) and omits estimation of fluxes, we focus our comparison on values presented in T-2009.

Spatial differences between the climatology created from surface water ΔfCO_2 values using the methods discussed above and the approach of T-2009 (3 million observations) are shown in Figure 7 for months February and August. months were selected for consistency with past comparisons presented in T-2009 and T-2002. The differences between this updated release and previous versions producing climatologies for reference years 2000 (T-2009) and 1990 (T-1997) are unlikely to represent real change in the oceans over time, but instead primarily reflect the impact of the greatly expanded database as well as the use of the ΔfCO_2 approach as opposed to the time normalization method of T-2009 (Supplementary Figure 9).

Deleted:).

Deleted: ; since

Deleted: ;

Deleted: .

The most significant regional differences between this updated version and that of T-2009 are observed over the subpolar North Atlantic, the subtropical Southeast Pacific and portions of the Southern Ocean. In the North Atlantic, differences between versions are largest in the boreal winter (February map, top panel of Figure 7) when the updated climatology exhibits less uptake compared to the T-2009 version (positive values on the map indicate more negative values in the T-2009 version). Differences in the North Atlantic can be at least partially attributed to the much greater availability of observations in this region between the two databases (Figure 1, Supplementary Figure 1, Supplementary Figure 9). This is discussed in further detail in the supplementary text.

The Southeast Pacific is an area with very limited observations but where a few key datasets have been included in the SOCAT database since 2010. Figure 1 shows that despite these recent additions to SOCAT, there are still only a few observations covering this region. Comparison of Figure 3 in this study with Figure 9 of T-2009 suggests that the additional datasets in SOCATv2022 result in a more defined seasonal cycle for fCO_2 in the subtropical Southeast Pacific in the current release. Specifically, the map of differences shown in Figure 7 shows that this region is a greater source of carbon to the atmosphere in austral summer and a greater sink in austral winter compared to T-2009 (compare also Figure 6 of this study with Figure 15 of T-2009). In contrast, monthly maps included in Figure 3 of T-2009 show little seasonal contrast in ΔpCO_2 likely due to a lack of observations.

In the Southern Ocean region during austral winter (August), ΔfCO_2 values are more negative in the current version compared to T-2009. The Southern Ocean is also a region of limited data availability particularly in austral winter but one where SOCATv2022 also includes several datasets added in the past decade that have an outsized influence on the resulting climatology.

Deleted:).

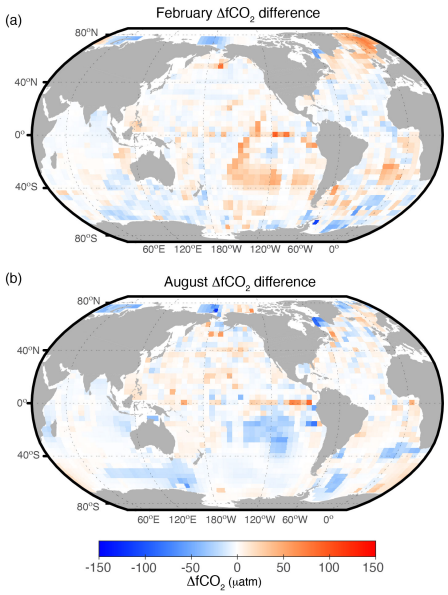

Figure 7: Difference maps for the surface water ΔfCO_2 climatology produced by this study using SOCAT and that from T-2009 (maps show this study *minus* T-2009) in (a) February and (b) August. In T-2009, the delta CO_2 values are reported as pCO_2 and here we are using fCO_2.

5.2 Comparison to other flux estimates

The estimate presented here for annual global mean carbon flux (-1.79 PgC yr^{-1}) represents slightly less uptake than reported by other studies, but given uncertainties, as well as differing timeframes, spatial coverage and gap-filling methodologies, our estimate compares closely with current estimates similarly based on observed surface ocean fCO_2.

To compare our new climatological estimate of contemporary air–sea net flux from surface ocean fCO_2 with estimates of the anthropogenic carbon flux from interior data (e.g., Gruber et al. 2019) or estimates from global ocean biogeochemical models (e.g., Friedlingstein et al. 2022; Hauck et al. 2020), it is necessary to account for the outgassing of natural carbon supplied to the ocean by rivers. This riverine estimate varies significantly in magnitude between studies and continues to be a research focus for the ocean carbon community. Therefore, we focus on comparisons between our

climatological estimate and a mean carbon flux estimate from an ensemble of observation-based pCO_2 products included in the SeaFlux product (Fay & Gregor et al. 2021).

The SeaFlux products span the years 1985-2020, are all similarly based on the SOCAT database, but employ various methods of machine learning and interpolation to produce full coverage ocean carbon maps. For this comparison, a climatology of the SeaFlux product is produced and fluxes are calculated in the same manner as for the climatology presented here. Following this approach, the SeaFlux climatology ensemble yields a global mean flux of -2.10 PgC yr^{-1} which represents a slightly larger flux into the ocean than that produced by the updated climatology (-1.79 ± 0.7 PgC yr^{-1}). The differences in global flux can be attributed to the true global coverage of the SeaFlux product relative to the 90% global ocean coverage of this study. As mentioned above in Section 4.2, an estimate of missing coastal and high latitude fluxes increases the ocean carbon uptake estimate for this climatology by roughly 0.38 PgC yr^{-1}. Adding this additional flux brings our analysis within 0.1 PgC yr^{-1} of the SeaFlux ensemble (-2.17 PgC yr^{-1} versus -2.10 PgC yr^{-1} for this analysis versus the SeaFlux estimate, respectively).

Spatially, comparison of the SeaFlux ensemble of products to our climatology shows strong agreement in overall patterns but significant differences in the mid and high latitude Southern Hemisphere oceans (Figure 8). Gloege et al. (2021) analyzed a machine learning method's ability to reconstruct global carbon fluxes from available observations using a testbed approach and found the highest flux bias in the Southern Ocean regions as well as an overestimation of decadal variability in this region. Given the limited availability of year-round observations at high Southern Hemisphere latitudes, and the resulting reliance on various gap-filling approaches, it is not surprising that the largest differences between the climatology presented here and the SeaFlux ensemble emerges in this region. Significant differences between these climatologies are also evident in the high latitude North Pacific and North Atlantic, specifically in the boreal winter season (Figure 8a). Again, a lack of observations in these regions during the winter season (Figure 1) likely accounts for much of this disagreement, with more reliance on the interpolation methods used by each method. Machine learning methods that utilize proxy variables to estimate pCO_2 in unsampled areas, such as those in the SeaFlux product, often rely on relationships derived from better-observed areas that are deemed similar in biogeochemical characteristics and it is likely that the mechanisms at these high latitude locations are not accurately captured by any available interpolation methods. This is also a current focus of research for the ocean carbon observing community.

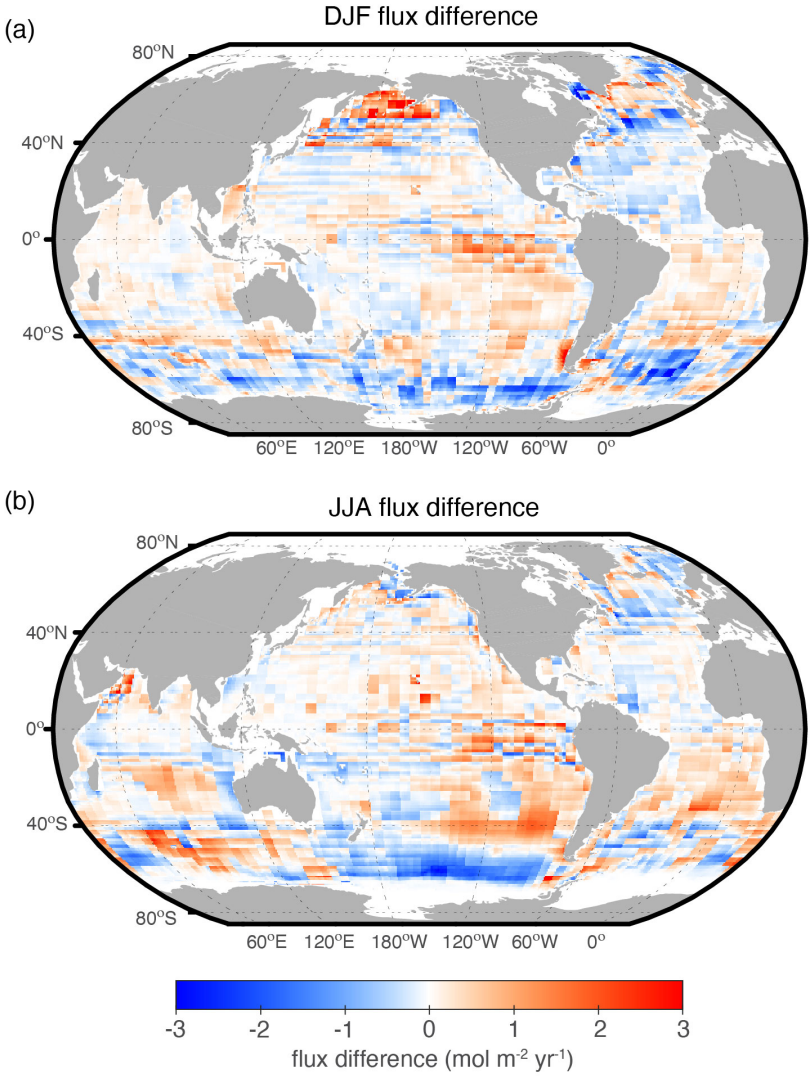

Figure 8: Difference map for carbon fluxes (mol m^{-2} yr^{-1}) calculated from this ΔfCO_2 climatology and fluxes reported by an ensemble of observation-based products included in the SeaFlux product for (a) boreal winter, DJF and (b) boreal summer, JJA. Map shows the difference defined as this study *minus* SeaFlux. Note that white areas at the poles are due to ice coverage extent (and therefore no value reported in the climatology) and not a flux difference of 0.

6. Conclusion

An updated climatological mean distribution for ΔfCO_2 (surface water minus atmosphere) using the methods of T-2009 is presented. This climatology is based on approximately seven times more open ocean observations from the SOCATv2022 database (over 21 million values, spanning years 1980-2021) compared to the 3 million data values used in T-2009 (and more than three times the approximately 6.5 million observations used in T-2014). In this updated climatology, observations made during El Niño periods over the equatorial Pacific are included, unlike climatologies presented by T-1997, T-2002, T-2009 and T-2014. In addition to coastal waters, the highest latitudes of the Arctic and the Mediterranean Sea are also excluded as in all previous LDEO climatologies.

To develop a climatology from data collected over multiple decades during which fCO_2 experienced a large secular trend, we calculate ΔfCO_2 values for each day and grid cell before collapsing all available data onto one climatological year. This method follows the assumption made in previous iterations of this climatology (T-1997) that the ocean surface carbon value follows the rate of increase in the atmospheric fCO_2, such that ΔfCO_2 is constant over time. Observed ΔfCO_2 is then interpolated in space-time using a lateral two-dimensional diffusion–advection equation on a 4ºx5º grid (Takahashi et al. 1995, T-1997, T-2002, T-2009, T-2014). Monthly mean ΔfCO_2 values for each pixel, downscaled to 1ºx1º resolution, are presented here. Net sea-air CO_2 flux is computed using the pySeaFlux package, following the protocol presented in Fay & Gregor et al. (2021).

Regional mean ΔfCO_2 values vary greatly among the ocean basins (Figures 3 and 4). The high-latitude North Atlantic is the most intense CO_2 sink per unit area as a result of both highly negative ΔfCO_2 (Figure 3) and strong winds. This is also the region with the largest differences between the climatologies created with previous versions of the LDEO database and this version based on the SOCATv2022 database (Figures 3 and 7). Globally, differences are due to the greater abundance of observations over all regions of the global oceans in the SOCAT database, but particularly the greater seasonal coverage in the Southern Hemisphere oceans and subpolar North Atlantic (Figure 1, Supplementary Figure 1).

The annual mean uptake flux for the global open-ocean region is estimated to be -1.79 ± 0.7 PgC yr^{-1} for 1980-2021 (Figures 5 and 6). Of the major ocean basins, the Southern Hemisphere ocean (south of 30S) is the largest CO_2 sink, taking up 1.22 PgC yr^{-1}, while the Northern Hemisphere ocean (north of 30N) takes up 0.93 PgC yr^{-1}. The

Deleted: oceans are

Deleted: 19

Deleted: oceans (subtropical and subpolar biomes) take

Deleted: 1.04

equatorial ocean region acts as the only year-round region of carbon efflux to the atmosphere and emits 0.36 PgC to the atmosphere annually.

While over a million new shipboard fCO_2^{oce} observations have been made each year in the global oceans for the past two decades, there has been a notable decline in the observations submitted to SOCAT since 2017 (Bakker et al. 2022, 2023). This decline is due in part to the disruption of the COVID19 pandemic, but also reflects a shift away from shipboard pCO_2 measurements. Given the lack of alternative approaches with which to assess spatial and temporal variability in air-sea CO_2 flux and the need for high accuracy shipboard measurements (accuracy of <2 µatm) to characterize most regions of the global oceans, this trend to fewer observations is highly detrimental to carbon cycle research. This is true both in regard to monitoring of ocean carbon uptake and to monitoring of more uncertain fluxes such as that between the atmosphere and terrestrial biosphere since the high uncertainty of independent terrestrial estimates necessitates the monitoring of this flux by difference.

Deleted: oceans act
Deleted: with
Deleted: emit
Deleted: 35
Deleted: yr^{-1}
Deleted: .
Deleted: .

Data Availability

The updated climatology is available via The National Center for Environmental Information (NCEI) at https://www.ncei.noaa.gov/access/metadata/landing-page/bin/iso?id=gov.noaa.nodc:028225, doi.org/10.25921/295g-sn13, (Fay et al. 2023).

Author contribution

ARF and DRM conducted the analysis and prepared the manuscript. GAM, RW, CW, SCS, and DP contributed ideas and provided feedback throughout the analysis as well as contributed to manuscript.

Acknowledgements

The Surface Ocean CO_2 Atlas (SOCAT) is an international effort, endorsed by the International Ocean Carbon Coordination Project (IOCCP), the Surface Ocean Lower Atmosphere Study (SOLAS) and the Integrated Marine Biosphere Research (IMBeR) program, to deliver a uniformly quality-controlled surface ocean CO_2 database. The many researchers and funding agencies responsible for the collection of data and quality control are thanked for their contributions to SOCAT. Funding was obtained from the NOAA Office of Oceanic and Atmospheric Research (OAR) Global Ocean Monitoring and Observations (GOMO) program.

References

Atlas, R., Hoffman, R. N., Ardizzone, J., Leidner, S. M., Jusem, J.C., Smith, D. K., and Gombos, D.: A cross-calibrated, multi- platform ocean surface wind velocity product for meteorological and oceanographic applications, B. Am. Meteorol. Soc., 92, 157– 174, https://doi.org/10.1175/2010BAMS2946.1, 2011.

Ayers, J.M. and Lozier, M.S., Unraveling dynamical controls on the North Pacific carbon sink. Journal of Geophysical Research: Oceans, 117(C1), 2012.

Bates, N. R., Astor, Y. M., Church, M. J., Currie, K., Dore, J. E., Gonzalez-Davila, M., Lorenzoni, L., Muller-Karger, F., Olafsson, J., & Santana-Casiano, J. M., A Time-Series View of Changing Surface Ocean Chemistry Due to Ocean Uptake of Anthropogenic CO_2 and Ocean Acidification. Oceanography, 27(1), 126–141. http://www.jstor.org/stable/24862128 2014.

Bakker, D. C. E., Pfeil, B. Landa, C. S., Metzl, N., O'Brien, K. M., Olsen, A., Smith, K., Cosca, C., Harasawa, S., Jones, S. D., Nakaoka, S., Nojiri, Y., Schuster, U., Steinhoff, T., Sweeney, C., Takahashi, T., Tilbrook, B., Wada, C., Wanninkhof, R., Alin, S. R., Balestrini, C. F., Barbero, L., Bates, N. R., Bianchi, A. A., Bonou, F., Boutin, J., Bozec, Y., Burger, E. F., Cai, W.-J., Castle, R. D., Chen, L., Chierici, M., Currie, K., Evans, W., Featherstone, C., Feely, R. A., Fransson, A., Goyet, C., Greenwood, N., Gregor, L., Hankin, S., Hardman-Mountford, N. J., Harlay, J., Hauck, J., Hoppema, M., Humphreys, M. P., Hunt, C. W., Huss, B., Ibánhez, J. S. P., Johannessen, T., Keeling, R., Kitidis, V., Körtzinger, A., Kozyr, A., Krasakopoulou, E., Kuwata, A., Landschützer, P., Lauvset, S. K., Lefèvre, N., Lo Monaco, C., Manke, A., Mathis, J. T., Merlivat, L., Millero, F. J., Monteiro, P. M. S., Munro, D. R., Murata, A., Newberger, T., Omar, A. M., Ono, T., Paterson, K., Pearce, D., Pierrot, D., Robbins, L. L., Saito, S., Salisbury, J., Schlitzer, R., Schneider, B., Schweitzer, R., Sieger, R., Skjelvan, I., Sullivan, K. F., Sutherland, S.

Deleted: Antonov, J. I., Locarnini, R. A., Boyer, T. P., Mishonov, A. V., and Garcia, H. E.: World Ocean Atlas 2005, in: Volume 2: Salinity, edited by: Levitus, S., NOAA Atlas NESDIS 62, US Government Printing Office, Washington, DC, 182 pp., 2006¶
¶

C., Sutton, A. J., Tadokoro, K., Telszewski, M., Tuma, M., Van Heuven, S. M. A. C., Vandemark, D., Ward, B., Watson, A. J., Xu, S.: A multi-decade record of high quality fCO2 data in version 3 of the Surface Ocean CO2 Atlas (SOCAT). Earth System Science Data 8: 383-413. doi:10.5194/essd8-383-2016, 2016.

Bakker, D. C. E.; Alin, S. R.; Becker, M.; Bittig, H. C.; Castaño-Primo, R.; Feely, R. A.; Gkritzalis, T.; Kadono, K.; Kozyr, A.; Lauvset, S. K.; Metzl, N.; Munro, D.R.; Nakaoka, S.; Nojiri, Y.; O'Brien, K. M.; Olsen, A.; Pfeil, B.; Pierrot, D.; Steinhoff, T.; Sullivan, K. F.; Sutton, A. J.; Sweeney, C.; Tilbrook, B.; Wada, C.; Wanninkhof, R.; Willstrand Wranne, A.; Akl, J.; Apelthun, L.B.; Bates, N.; Beatty, C.M.; Burger, E. F.; Cai, W.; Cosca, C.E.; Corredor, J.E.; Cronin, M.; Cross, J. N.; De Carlo, E. H.; DeGrandpre, M. D.; Emerson, S. R.; Enright, M. P.; Enyo, K.; Evans, W.; Frangoulis, C.; Fransson, A.; García-Ibáñez, M. I.; Gehrung, M.; Giannoudi, L.; Glockzin, M.; Hales, B.; Howden, S.D.; Hunt, C. W.; Ibánhez, J.S. P.; Jones, S. D.; Kamb, L.; Körtzinger, A.; Landa, C. S.; Landschützer, P.; Lefèvre, N.; Lo Monaco, C.; Macovei, V. A.; Maenner, A.; Jones, S.; Meinig, C.; Millero, F. J.; Monacci, N. M.; Mordy, C.; Morell, J. M.; Murata, A.; Musielewicz, S.; Neill, C.; Newberger, T.; Nomura, D.; Ohman, M.; Ono, T.; Passmore, A.; Petersen, W.; Petihakis, G.; Perivoliotis, L.; Plueddemann, A. J.; Rehder, G.; Reynaud, T.; Rodriguez, C.; Ross, A. C.; Rutgersson, A.; Sabine, C. L.; Salisbury, J. E.; Schlitzer, R.; Send, U.; Skjelvan, I.; Stamataki, N.; Sutherland, S.C.; Tadokoro, K.; Tanhua, T.; Telszewski, M.; Trull, T.; Vandemark, D.; van Ooijen, E.; Voynova, Y. G.; Wang, H.; Weller, R. A.; Whitehead, C.s; Wilson, D. (2022). Surface Ocean CO2 Atlas Database Version 2022 (SOCATv2022) (NCEI Accession 0253659). NOAA National Centers for Environmental Information. Dataset. https://doi.org/10.25921/1h9f-nb73. Accessed July 14, 2022.

Bakker, D., Sanders, R., Collins, A., DeGrandpre, M., Gkritzalis, T., Ibánhez, S., Jones, S., Lauvset, S., Metzl, N., O'Brien, K., Olsen, A., Schuster, U., Steinhoff, T., Telszewski, M., Tilbrook, B., Wallace, D.: Case for SOCAT as an integral part of the value chain advising UNFCCC on ocean CO2 uptake http://www.ioccp.org/images/Gnews/2023_A_Case_for_SOCAT.pdf, 2023

Chen, C. T. A., and S. Tsunogai. "Carbon and nutrients in the ocean." Asian Change in the Context of Global Change: 271-307, 1998.

DeVries T., Yamamoto K., Wanninkhof R., Gruber N., Hauck J., Müller J.D., Bopp L., Carroll D., Carter B., Chau T., Doney S., Gehlen M., Gloege L., Gregor L., Henson S., Kim J.H., Iida Y., Ilyina T., Landschützer P., Le Quéré C., Munro D., Nissen C., Patara L., Perez F.F., Resplandy L., Rodgers K., Schwinger J., Séférian R., Sicardi V., Terhaar J., Triñanes J., Tsujino H., Watson A., Yasunaka S., Zeng, J.: Magnitude, trends, and variability of the global ocean carbon sink from 1985-2018, Global Biogeochemical Cycles, 37, e2023GB007780. https://doi.org/10.1029/2023GB007780, 2023.

Deleted: Simone…. R.; Becker, Meike;….; Bittig, Henry…. C.; Castaño-Primo, Rocío;….; Feely, Richard…. A.; Gkritzalis, Thanos;….; Kadono, Koji;….; Kozyr, Alex;….; Lauvset, Siv…. K.; Metzl, Nicolas;….; Munro, David ….R.; Nakaoka, Shin-ichiro;….; Nojiri, Yukihiro;….; O'Brien, Kevin…. M.; Olsen, Are;….; Pfeil, Benjamin;….; Pierrot, Denis;….; Steinhoff, Tobias;….; Sullivan, Kevin…. F.; Sutton, Adrienne…. J.; Sweeney, Colm;….; Tilbrook, Bronte;….; Wada, Chisato;….; Wanninkhof, Rik;….; Willstrand Wranne, Anna;….; Akl, John;….; Apelthun, Lisa ….B.; Bates, Nicholas;….; Beatty, Cory ….M.; Burger, Eugene…. F.; Cai, Wei-Jun;….; Cosca, Catherine ….E.; Corredor, Jorge ….E.; Cronin, Margot;….; Cross, Jessica…. N.; De Carlo, Eric…. H.; DeGrandpre, Michael…. D.; Emerson, Steven…. R.; Enright, Matt…. P.; Enyo, Kazutaka;….; Evans, Wiley;….; Frangoulis, Constantin;….; Fransson, Agneta;….; García-Ibáñez, Maribel…. I.; Gehrung, Martina;….; Giannoudi, Louisa;….; Glockzin, Michael;….; Hales, Burke;….; Howden, Stephan ….D.; Hunt, Christopher…. W.; Ibánhez, J. Severino…. P.; Jones, Steve…. D.; Kamb, Linus;….; Körtzinger, Arne;….; Landa, Camilla…. S.; Landschützer, Lefèvre, Nathalie;….; Lo Monaco, Claire;….; Macovei, Vlad…. A.; Maenner, A.; Jones, Stacy;….; Meinig, Christian;….; Millero, Frank…. J.; Monacci, Natalie…. M.; Mordy, Calvin;….; Morell, Julio…. M.; Murata, Akihiko;….; Musielewicz, Sylvia;….; Neill, Craig;….; Newberger, Tim;….; Nomura, Daiki;….; Ohman, Mark;….; Ono, Tsuneo;….; Passmore, Abe;….; Petersen, Wilhelm;….; Petihakis, George;….; Perivoliotis, Leonidas;….; Plueddemann, Albert…. J.; Rehder, Gregor;….; Reynaud, Thierry;….; Rodriguez, Carmen;….; Ross, Andrew…. C.; Rutgersson, Anna;….; Sabine, Christopher…. L.; Salisbury, Joseph…. E.; Schlitzer, Reiner;….; Send, Uwe;….; Skjelvan, Ingunn;….; Stamataki, Natalia;….; Stewart ….C.; Sweeney, Colm;…Tadokoro, Kazuaki;….; Tanhua, Toste;….; Telszewski, Maciej;….; Trull, Tom;….; Vandemark, Douglas;….; van Ooijen, Erik;….; Voynova, Yoana…. G.; Wang, Hongjie;….; Weller, Robert…. A.; Whitehead, Chris….s; Wilson, Doug… ... [1]

Deleted: submitted to

Dickson, A. G., Sabine, C. L., and Christian, J. R. (Eds.): Guide to best practices for ocean CO2 measurements, PICES Special Publication 3, IOCCP Report 8, 191 pp., 2007.

Fay, A.R. and McKinley, G.A.: Global trends in surface ocean pCO2 from in situ data. Global Biogeochemical Cycles, 27(2), pp.541-557, 2013.

Fay, A. R., & McKinley, G. A.: Global open-ocean biomes: Mean and temporal variability. Earth System Science Data, 6(2), 273–284. https://doi.org/10.5194/essd-6-273-2014, 2014.

Fay, A. R., Gregor, L., Landschützer, P., McKinley, G. A., Gruber, N., Gehlen, M., Iida, Y., Laruelle, G. G., Rödenbeck, C., Roobaert, A., and Zeng, J.: SeaFlux: harmonization of air–sea CO2 fluxes from surface pCO2 data products using a standardized approach, Earth Syst. Sci. Data, 13, 4693–4710, https://doi.org/10.5194/essd-13-4693-2021, 2021

Fay, A. R., Munro, D.R., McKinley, G. A., Pierrot, D., Sutherland, S. C., Sweeney, C., Wanninkhof, R.: Climatological distributions of sea-air Delta fCO2 and CO2 flux densities in the Global Surface Ocean (NCEI Accession 0282251). NOAA National Centers for Environmental Information. Dataset. https://doi.org/10.25921/295g-sn13, 2023.

Feng, S., Lauvaux, T., Keller, K., Davis, K. J., Rayner, P., Oda, T., and Gurney, K. R.: A road map for improving the treatment of uncertainties in high-resolution regional carbon flux inverse estimates, Geophysical Research Letters, 46, 13,461–13,469. https://doi.org/10.1029/2019GL082987, 2019.

Friedlingstein, P., O'Sullivan, M., Jones, M. W., Andrew, R. M., Gregor, L., Hauck, J., Le Quéré, C., Luijkx, I. T., Olsen, A., Peters, G. P., Peters, W., Pongratz, J., Schwingshackl, C., Sitch, S., Canadell, J. G., Ciais, P., Jackson, R. B., Alin, S. R., Alkama, R., Arneth, A., Arora, V. K., Bates, N. R., Becker, M., Bellouin, N., Bittig, H. C., Bopp, L., Chevallier, F., Chini, L. P., Cronin, M., Evans, W., Falk, S., Feely, R. A., Gasser, T., Gehlen, M., Gkritzalis, T., Gloege, L., Grassi, G., Gruber, N., Gürses, Ö., Harris, I., Hefner, M., Houghton, R. A., Hurtt, G. C., Iida, Y., Ilyina, T., Jain, A. K., Jersild, A., Kadono, K., Kato, E., Kennedy, D., Klein Goldewijk, K., Knauer, J., Korsbakken, J. I., Landschützer, P., Lefèvre, N., Lindsay, K., Liu, J., Liu, Z., Marland, G., Mayot, N., McGrath, M. J., Metzl, N., Monacci, N. M., Munro, D. R., Nakaoka, S.-I., Niwa, Y., O'Brien, K., Ono, T., Palmer, P. I., Pan, N., Pierrot, D., Pocock, K., Poulter, B., Resplandy, L., Robertson, E., Rödenbeck, C., Rodriguez, C., Rosan, T. M., Schwinger, J., Séférian, R., Shutler, J. D., Skjelvan, I., Steinhoff, T., Sun, Q., Sutton, A. J.,

Sweeney, C., Takao, S., Tanhua, T., Tans, P. P., Tian, X., Tian, H., Tilbrook, B., Tsujino, H., Tubiello, F., van der Werf, G. R., Walker, A. P., Wanninkhof, R., Whitehead, C., Willstrand Wranne, A., Wright, R., Yuan, W., Yue, C., Yue, X., Zaehle, S., Zeng, J., and Zheng, B.: Global Carbon Budget 2022, Earth Syst. Sci. Data, 14, 4811–4900, https://doi.org/10.5194/essd-14-4811-2022, 2022.

Gloege, L., McKinley, G. A., Landschutzer, P., Fay, A. R., Frol- icher, T., Fyfe, J., Ilyina, T., Jones, S., Lovenduski, N. S., Röden- beck, C., Rogers, K., Schlunegger, S., and Takano, Y.: Quantifying errors in observationally-based estimates of ocean carbon sink variability, Global Biogeochem. Cy., 35, e2020GB006788, https://doi.org/10.1029/2020GB006788, 2021.

Good, S. A., Martin, M. J., and Rayner, N. A.: EN4: Quality controlled ocean temperature and salinity pro- files and monthly objective analyses with uncertainty estimates, J. Geophys. Res.-Oceans, 118, 6704–6716, https://doi.org/10.1002/2013JC009067, 2013.

Gregor L., & Fay, A. R.: SeaFlux data set: harmonised sea-air CO2 fluxes from surface pCO2 data products using a standardised approach (2021.04, Data set: Zenodo. https://doi.org/10.5281/zenodo.5148460, 2021. Last accessed September, 12, 2022.

Gruber, N., Clement, D., Carter, B. R., Feely, R. A., van Heuven, S., Hoppema, M., et al.: The oceanic sink for anthropogenic co2 from 1994 to 2007. Science 363, 1193–1199. doi: 10.1126/science.aau5153, 2019.

Gruber, N., Bakker, D. C., DeVries, T., Gregor, L., Hauck, J., Landschützer, P., ... & Müller, J. D.: Trends and variability in the ocean carbon sink. Nature Reviews Earth & Environment, 4(2), 119-134, 2023.

Hauck, J., Zeising, M., Le Quéré, C., Gruber, N., Bakker, D. C. E.,Bopp, L., Chau, T. T. T., Gürses, Ö., Ilyina, T., Landschützer, P., Lenton, A., Resplandy, L., Rödenbeck, C., Schwinger, J., and Séférian, R.: Consistency and Challenges in the Ocean Carbon Sink Estimate for the Global Carbon Budget, Front. Mar. Sci., 7, 852-885, https://doi.org/10.3389/fmars.2020.571720, 2020.

Hersbach, H., Bell, B., Berrisford, P., Hirahara, S., Horányi, A., Muñoz-Sabater, J., Nicolas, J., Peubey, C., Radu, R., Schepers, D., Simmons, A., Soci, C., Abdalla, S., Abellan, X., Balsamo, G., Bechtold, P., Biavati, G., Bidlot, J., Bonavita, M., De Chiara, G., Dahlgren, P., Dee, D., Diamantakis, M., Dragani, R., Flemming, J., Forbes, R., Fuentes, M., Geer, A., Haimberger, L., Healy, S., Hogan, R.J., Hólm, E., Janisková, M., Keeley, S., Laloyaux, P., Lopez, P., Lupu, C., Radnoti, G., de Rosnay, P., Rozum, I.,

Vamborg, F., Villaume, S., and Thépaut, J.: The ERA5 global reanalysis, Q. J. Roy. Meteor. Soc. 146, 1999–2049, https://doi.org/10.1002/qj.3803, 2020 (data available at: https://cds.climate.copernicus.eu/cdsapp#!/dataset/ reanalysis-era5-single-levels-monthly-means?tab=overview, last access: 16 October, 2020).

Jacobson, A. R., Mikaloff-Fletcher, S. E., Gruber, N., Sarmiento, J. S., and Gloor, M.: A joint atmosphere-ocean inver- sion for surface fluxes of carbon dioxide: 1. Methods and global-scale fluxes, Glob. Biogeochem. Cy., 21, GB1019, doi:10.1029/2005GB002556, 2007.

Ho, D. T., Wanninkhof, R., Schlosser, P., Ullman, D. S., Hebert, D., and Sullivan, K. F.: Towards a universal relationship between wind speed and gas exchange: Gas transfer ve- locities measured with 3He/SF6 during the Southern Ocean Gas Exchange Experiment, J Geophys. Res., 116, C00F04, doi:10.1029/2010JC006854, 2011.

Kalnay, E., Kanamitsu, M., Kistler, R., Collins, W., Deaven, D., Gandin, L., Iredell, M., Saha, S., White, G.,Woollen, J., Zhu, Y., Chelliah, M., Ebisuzaki, W., Higgins, W., Janowiak, J., Mo, K. C., Ropelewski, C., Wang, J., Leetmaa, A., Reynolds, R., Jenne, R., and Joseph, D.: The NCEP/NCAR 40-year reanalysis project, B. Am. Meteorol. Soc., 77, 437–470, 1996.

Kobayashi, S., Ota, Y., Harada, Y., Ebita, A., Moriya, M., Onoda, H., Onogi, K., Kamahori, H., Kobayashi, C., Endo, H., Miyaoka, K., and Takahashi, K.: The JRA-55 Reanalysis: General Spec- ifications and Basic Characteristics, J. Meteorol. Soc. Jpn., 93, 5–48, https://doi.org/10.2151/jmsj.2015-001, 2015.

Lan, X., Tans, P., Thoning, K., & NOAA Global Monitoring Laboratory. NOAA Greenhouse Gas Marine Boundary Layer Reference - CO2. [Data set]. NOAA GML. https://doi.org/10.15138/DVNP-F961, 2023.

Landschützer, P., Gruber, N. and Bakker, D.C.: Decadal variations and trends of the global ocean carbon sink. Global Biogeochemical Cycles, 30(10), pp.1396-1417, 2016.

Landschützer, P., Laruelle, G. G., Roobaert, A., and Regnier, P.: A uniform pCO2 climatology combining open and coastal oceans, Earth Syst. Sci. Data, 12, 2537–2553, https://doi.org/10.5194/essd-12-2537-2020, 2020.

Manning, A. C., and Keeling, R. F., Global oceanic and land biotic carbon sinks from the Scripps atmospheric oxygen flask sampling network, Tellus, 58B, pp. 95-116, 2006.

Deleted:

McKinley, G.A., Fay, A.R., Eddebbar, Y.A., Gloege, L. and Lovenduski, N.S.: External forcing explains recent decadal variability of the ocean carbon sink. Agu Advances, 1(2), p.e2019AV000149, 2020.

Pfeil, B., Olsen, A., Bakker, D. C. E., Hankin, S., Koyuk, H., Kozyr, A., Malczyk, J., Manke, A., Metzl, N., Sabine, C. L., Akl, J., Alin, S. R., Bates, N., Bellerby, R. G. J., Borges, A., Boutin, J., Brown, P. J., Cai, W.-J., Chavez, F. P., Chen, A., Cosca, C., Fassbender, A. J., Feely, R. A., González-Dávila, M., Goyet, C., Hales, B., Hardman-Mountford, N., Heinze, C., Hood, M., Hoppema, M., Hunt, C. W., Hydes, D., Ishii, M., Johannessen, T., Jones, S. D., Key, R. M., Körtzinger, A., Landschützer, P., Lauvset, S. K., Lefèvre, N., Lenton, A., Lourantou, A., Merlivat, L., Midorikawa, T., Mintrop, L., Miyazaki, C., Murata, A., Nakadate, A., Nakano, Y., Nakaoka, S., Nojiri, Y., Omar, A. M., Padin, X. A., Park, G.-H., Paterson, K., Perez, F. F., Pierrot, D., Poisson, A., Rios, A. F., Santana-Casiano, J. M., Salisbury, J., Sarma, V. V. S. S., Schlitzer, R., Schneider, B., Schuster, U., Sieger, R., Skjelvan, I., Steinhoff, T., Suzuki, T., Takahashi, T., Tedesco, K., Telszewski, M., Thomas, H., Tilbrook, B., Tjiputra, J., Vandemark, D., Veness, T., Wanninkhof, R., Watson, A. J., Weiss, R., Wong, C. S., Yoshikawa-Inoue, H.: A uniform, quality controlled Surface Ocean CO2 Atlas (SOCAT) Earth System Science Data , 5, 125-143.doi:10.5194/essd-5-125-2013, 2013.

Quay, P. D., Tilbrook, B., and Wong C. S., Oceanic uptake of fossil fuel CO_2: carbon-13 evidence, Science, 256, pp. 74-79, 1992.

Reynolds, R. W., Rayner, N. A., Smith, T. M., Stokes, D. C., and Wang, W.: An improved in situ and satellite SST analysis for cli- mate, J. Climate, 15, 1609–1625, https://doi.org/10.1175/1520- 0442(2002)015<1609:AIISAS>2.0.CO;2, 2002 (data available at: https://psl.noaa.gov/data/gridded/data.noaa.oisst.v2.html, last access: 26 April 2021).

Ridge, S. M., & McKinley, G. A.: Advective Controls on the North Atlantic Anthropogenic Carbon Sink. Global Biogeochemical Cycles, 34(7), 1138. https://doi.org/10.1029/2019gb006457, 2020.

Rödenbeck, C., Bakker, D. C. E., Gruber, N., Iida, Y., Jacobson, A. R., Jones, S., Landschützer, P., Metzl, N., Nakaoka, S., Olsen, A., Park, G.-H., Peylin, P., Rodgers, K. B., Sasse, T. P., Schuster, U., Shutler, J. D., Valsala, V., Wanninkhof, R., and Zeng, J.: Data-based estimates of the ocean carbon sink variability – first results of the Surface Ocean pCO_2 Mapping intercomparison (SOCOM), Biogeosciences, 12, 7251–7278, https://doi.org/10.5194/bg-12-7251-2015, 2015.

Sabine, C. L., Wanninkhof, R., Key, R. M., Goyet, C., & Millero, F. J.:Seasonal CO2 fluxes in the tropical and subtropical Indian Ocean. Marine Chemistry, 72(1), 33–53. https://doi.org/10.1016/s0304-4203(00)00064-5, 2000.

Sabine, C. L., Hankin, S., Koyuk, H., Bakker, D. C. E., Pfeil, B., Olsen, A., Metzl, N., Kozyr, A., Fassbender, A., Manke, A., Malczyk, J., Akl, J., Alin, S. R., Bellerby, R. G. J., Borges, A., Boutin, J., Brown, P. J., Cai, W.-J., Chavez, F. P., Chen, A., Cosca, C., Feely, R. A., González-Dávila, M., Goyet, C., Hardman-Mountford, N., Heinze, C., Hoppema, M., Hunt, C. W., Hydes, D., Ishii, M., Johannessen, T., Key, R. M., Körtzinger, A., Landschützer, P., Lauvset, S. K., Lefèvre, N., Lenton, A., Lourantou, A., Merlivat, L., Midorikawa, T., Mintrop, L., Miyazaki, C., Murata, A., Nakadate, A., Nakano, Y., Nakaoka, S., Nojiri, Y., Omar, A. M., Padin, X. A., Park, G.-H., Paterson, K., Perez, F. F., Pierrot, D., Poisson, A., Ríos, A. F., Salisbury, J., Santana-Casiano, J. M., Sarma, V. V. S. S., Schlitzer, R., Schneider, B., Schuster, U., Sieger, R., Skjelvan, I., Steinhoff, T., Suzuki, T., Takahashi, T., Tedesco, K., Telszewski, M., Thomas, H., Tilbrook, B., Vandemark, D., Veness, T., Watson, A. J., Weiss, R., Wong, C. S., and Yoshikawa-Inoue, H.: Surface Ocean CO2 Atlas (SOCAT) gridded data products, Earth Syst. Sci. Data, 5, 145–153, https://doi.org/10.5194/essd-5-145-2013, 2013.

Takahashi, T., Olafsson, J., Goddard, J.G., Chipman, D.W. and Sutherland, S.C.: Seasonal variation of CO2 and nutrients in the high-latitude surface oceans: A comparative study. Global Biogeochemical Cycles, 7(4), pp.843-878, 1993.

Takahashi, T., Takahashi, T. T., & Sutherland, S. C.: An assessment of the role of the North Atlantic as a CO2 sink. Philosophical Transactions of the Royal Society of London. Series B: Biological Sciences, 348(1324), 143-152, 1995.

Takahashi, T., Feely, R.A., Weiss, R.F., Wanninkhof, R.H., Chipman, D.W., Sutherland, S.C. and Takahashi, T.T.: Global air-sea flux of CO2: An estimate based on measurements of sea–air pCO2 difference. Proceedings of the National Academy of Sciences, 94(16), pp.8292-8299, 1997.

Takahashi, T., Sutherland, S.C., Sweeney, C., Poisson, A., Metzl, N., Tilbrook, B., Bates, N., Wanninkhof, R., Feely, R.A., Sabine, C. and Olafsson, J.: Global sea–air CO2 flux based on climatological surface ocean pCO2, and seasonal biological and temperature effects. Deep Sea Research Part II: Topical Studies in Oceanography, 49(9-10), pp.1601-1622, 2002.

Takahashi, T.: "The fate of industrial carbon dioxide." Science 305, no. 5682: 352-353 2004.

Takahashi, T., Sutherland, S.C., Wanninkhof, R., Sweeney, C., Feely, R.A., Chipman, D.W., Hales, B., Friederich, G., Chavez, F., Sabine, C. and Watson, A., Bakker, D.C.E., Schuster U., Metzl, N., Yoshikawa-Inoue, H., Ishii, M., Midorikawa, T., Nojiri, Y., Körtzinger, A., Steinhoff, T., Hoppema, M., Olafsson, J., Arnarson, T.S., Tilbrook, B., Johannessen, T., Olsen, A., Bellerby, R., Wong, C.S., Delille, B., Bates, N.R., de Baar, H.J.W.: Climatological mean and decadal change in surface ocean pCO2, and net sea–air CO2 flux over the global oceans. Deep Sea Research Part II: Topical Studies in Oceanography, 56(8-10), pp.554-577, http://dx.doi.org/10.1016/j.dsr2.2008.12.009. 2009a.

Takahashi, T., Sutherland, S.C., Wanninkhof, R., Sweeney, C., Feely, R.A., Chipman, D.W., Hales, B., Friederich, G., Chavez, F., Sabine, C. and Watson, A., Bakker, D.C.E., Schuster U., Metzl, N., Yoshikawa-Inoue, H., Ishii, M., Midorikawa, T., Nojiri, Y., Körtzinger, A., Steinhoff, T., Hoppema, M., Olafsson, J., Arnarson, T.S., Tilbrook, B., Johannessen, T., Olsen, A., Bellerby, R., Wong, C.S., Delille, B., Bates, N.R., de Baar, H.J.W.:: Corrigendum to “Climatological mean and decadal change in surface ocean pCO2, and net sea–air CO2 flux over the global oceans.” Deep Sea Research Part I: Oceanographic Research Papers, 56(11), pp.2075-2076, https://doi.org/10.1016/j.dsr.2009.07.007, 2009b.

Takahashi, T., S. C. Sutherland, D. W. Chipman, J. G. Goddard, C. Ho, T. Newberger, C. Sweeney, and D. R. Munro: Climatological distributions of pH, pCO2, total CO2, alkalinity, and CaCO3 saturation in the global surface ocean, and temporal changes at selected locations, Mar. Chem., 164, 95–125, doi:10.1016/j.marchem.2014.06.004, 2014.

Takahashi, T.; Sutherland, S. C.; Kozyr, A.: Global Ocean Surface Water Partial Pressure of CO2 Database: Measurements Performed During 1957-2019 (LDEO Database Version 2019) (NCEI Accession 0160492). Version 9.9. NOAA National Centers for Environmental Information. Dataset. https://doi.org/10.3334/CDIAC/OTG.NDP088(V2015) Accessed March 15, 2021.

Tanhua, T., Orr, J. C., Lorenzoni L., and Hansson L.: WMO Bulletin nº : Vol 64 (1) - 2015 (available at https://public.wmo.int/en/resources/bulletin/monitoring-ocean-carbon-and-ocean-acidification-0), 2015.

Tans, P.p, Fung, I.Y., Takahashi, T., Observational Contrains on the Global Atmospheric Co2 Budget.Science247,1431-1438. DOI:10.1126/science.247.4949.1431, 1990.

Deleted: 2009

Deleted:

Tans, P.P., Berry, J.A., Keeling, R.F.: Oceanic 13C/12C observations: a new window on ocean CO2 uptake. Global Biogeochemical Cycles 7.2: 353-368, 1993.

Tjiputra, J.F., Olsen, A., Bopp, L., Lenton, A., Pfeil, B., Roy, T., Segschneider, J., Totterdell, I., Heinze, C.: Long-term surface pCO2 trends from observations and models, Tellus B: Chemical and Physical Meteorology, 66:1, 23083, DOI: 10.3402/tellusb.v66.23083, 2014.

Wanninkhof, R., Park, G.-H., Takahashi, T., Sweeney, C., Feely, R., Nojiri, Y., Gruber, N., Doney, S. C., McKinley, G. A., Lenton, A., Le Quéré, C., Heinze, C., Schwinger, J., Graven, H., and Khatiwala, S.: Global ocean carbon uptake: magnitude, variability and trends, Biogeosciences, 10, 1983–2000, https://doi.org/10.5194/bg-10-1983-2013, 2013.

Wanninkhof R.: Relationship between wind speed and gas exchange over the ocean revisited, Limnol. Oceanogr. Methods, 12, doi:10.4319/lom.2014.12.351, 2014.

Weiss, R.: Carbon dioxide in water and seawater: the solubility of non-ideal gas, Mar. Chem. 2, 203–215, https://doi.org/10.1016/0304-4203(74)90015-2, 1974.

Deleted:

Supplementary Figures

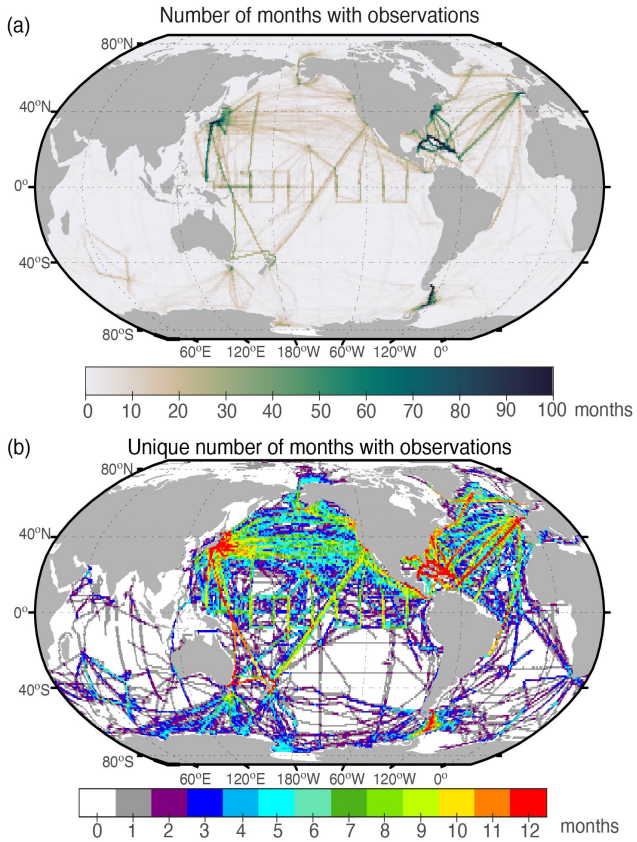

Supplementary Figure 1: (a) Total number of months with at least one observation in each 1º grid cell in the LDEOv2019 database, for years 1980-2019. The maximum number possible for a grid cell is 480 (40 years * 12 months). (b) the number of unique calendar months in each grid cell where at least one observation has been made since 1980. Red indicates grid cells where each month (Jan - Dec) has been sampled at least once over the 40 year time series while white indicates grid cells with no measurements over the length of the time series.

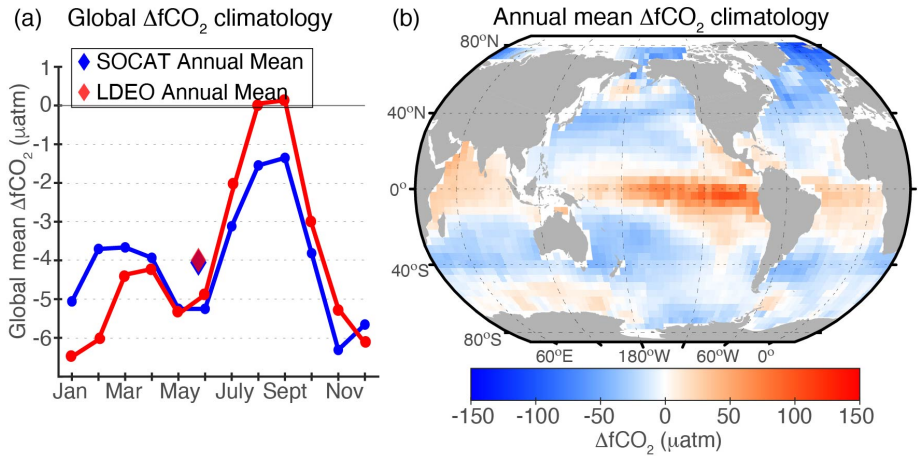

1660 Supplementary Figure 2: (a) Global mean delta fCO_2 seasonal climatology from the SOCATv2022 (blue) and LDEOv2019 (red) databases; annual mean values are indicated by the diamond (SOCATv2022 = -4.1 µatm and LDEOv2019 = -3.9). (b) Map of annual ΔfCO_2 climatology using LDEOv2019 database.

1665

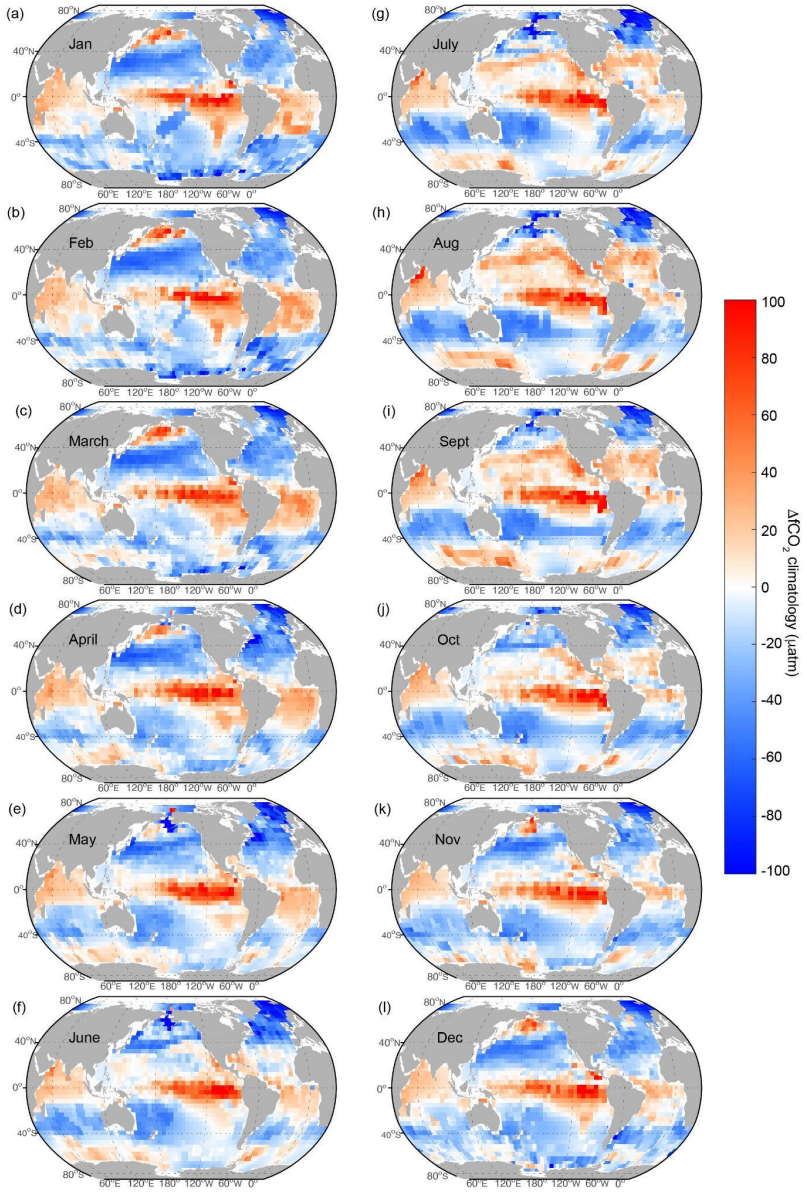

Supplementary Figure 3. Monthly mean values for sea–air ΔfCO_2 obtained using the
1670 LDEO database. Warm colors indicate positive ΔfCO_2 (ocean is greater than

atmospheric CO_2), white indicates near zero ΔfCO_2, and cool colors indicate negative ΔfCO_2 (ocean CO_2 is lower than the atmosphere).

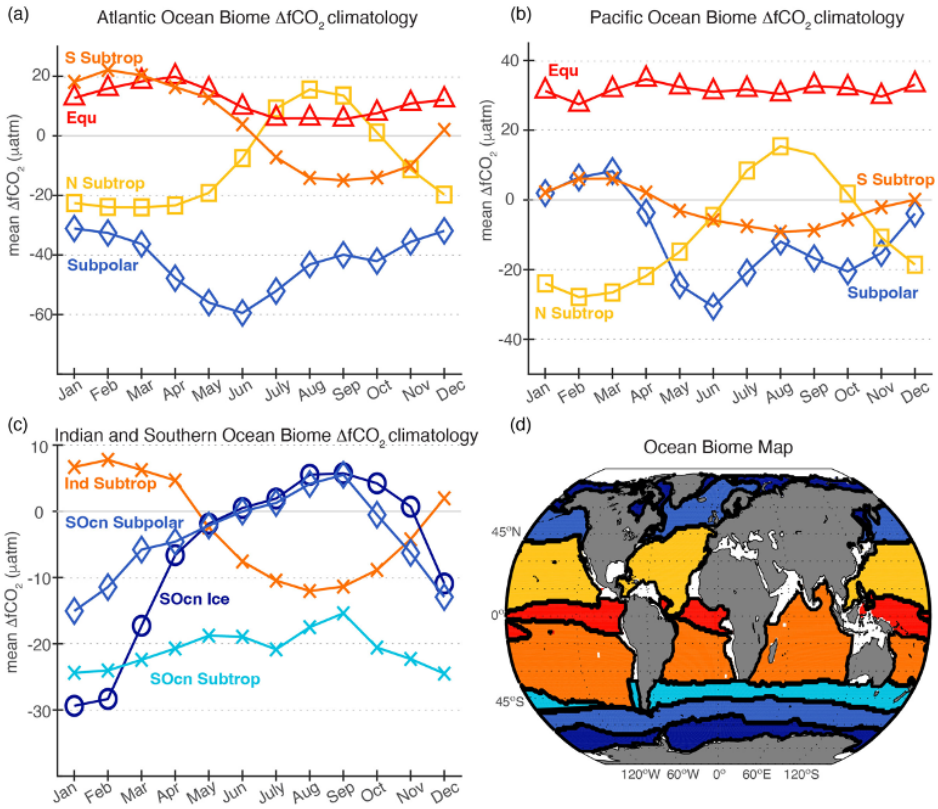

Supplementary Figure 4: Monthly climatology (produced using the LDEO database) of ΔfCO_2 for each regional ocean biome in the (a) Atlantic, (b) Pacific, (c) Indian and Southern Ocean basins. (d) Map of regional biomes. Colors of curves correspond to regions on the map in (d) with labels in matching colored text. Note that the y-axis varies between subplots.

Biome	DJF	MAM	JJA	SON
NP ICE	None (1)	-18.27 (3)	0.64 (20)	1.65 (20)
NP SPSS	2.1 (29)	0.99 (36)	0.94 (38)	1.76 (33)
NP STSS	1.62 (41)	1.38 (37)	1.78 (35)	2.05 (34)
NP STPS	1.49 (41)	1.45 (38)	2.14 (38)	1.94 (36)
W Pac Equ	1.36 (41)	1.38 (34)	1.64 (35)	1.75 (36)
E Pac Equ	2.57 (38)	1.97 (37)	2.04 (34)	2.36 (34)
SP STPS	1.06 (36)	0.54 (36)	0.45 (35)	0.41 (35)
NA ICE	1.38 (12)	0.42 (17)	1.92 (19)	1.82 (20)
NA SPSS	2.02 (27)	1.5 (32)	1.58 (32)	1.28 (31)
NA STSS	1.83 (29)	1.71 (30)	2.08 (31)	1.91 (34)
NA STPS	1.57 (30)	1.59 (28)	2.04 (28)	1.78 (34)
Atl Equ	1.37 (18)	1.49 (23)	1.41 (17)	1.71 (26)
SA STPS	1.69 (24)	1.88 (20)	1.64 (15)	1.58 (27)
IND	1.49 (29)	1.89 (17)	2.23 (17)	1.64 (14)
SO STSS	1.82 (34)	1.69 (32)	1.37 (32)	1.13 (33)
SO SPSS	1.67 (34)	1.77 (32)	1.88 (29)	1.71 (32)
SO ICE	0.87 (33)	1.00 (28)	1.77 (25)	2.64 (29)

Supplementary Table 1: Seasonal trends (µatm/yr) for biome-mean fCO_2 values- rows representing the 17 biomes as described in Fay & McKinley et al. 2014 and columns representing seasons (DJF: December, January, February; MAM: March, April, May, etc). Value in parentheses in each cell indicates the number of years with a biome mean value available in that season (max would be 42 as there are 42 years included in our analysis of 1980-2021).

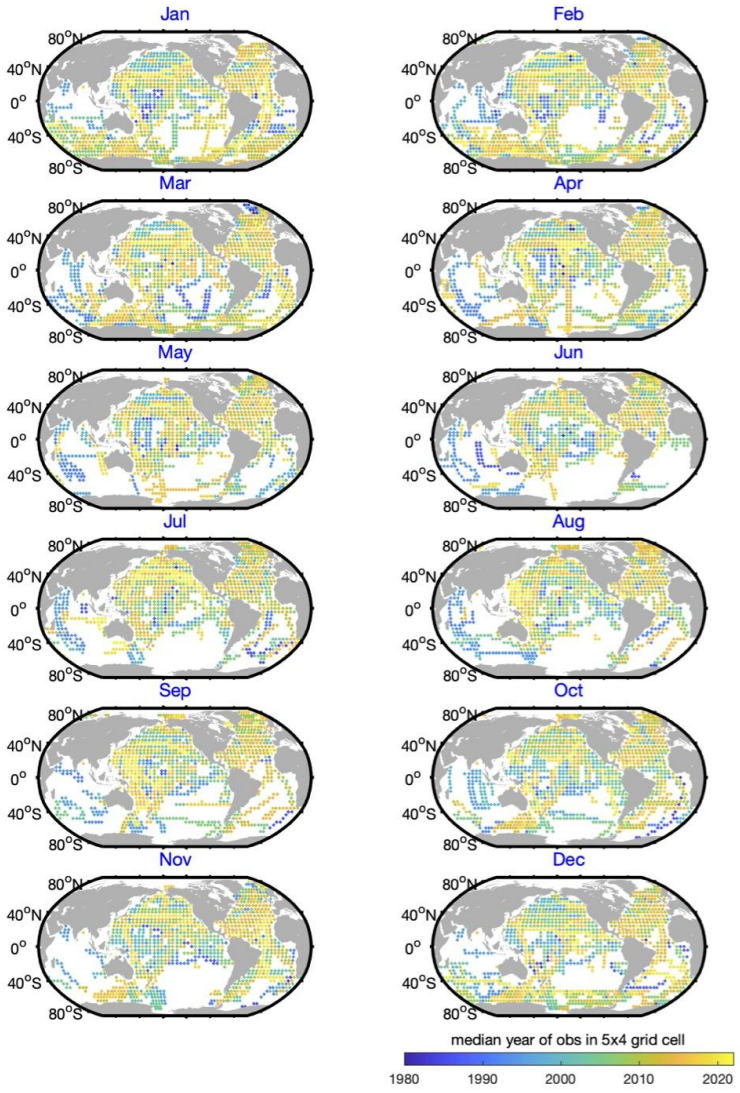

1695

Supplementary Figure 5: Median year of all observations feeding into this climatology, mapped for each month.

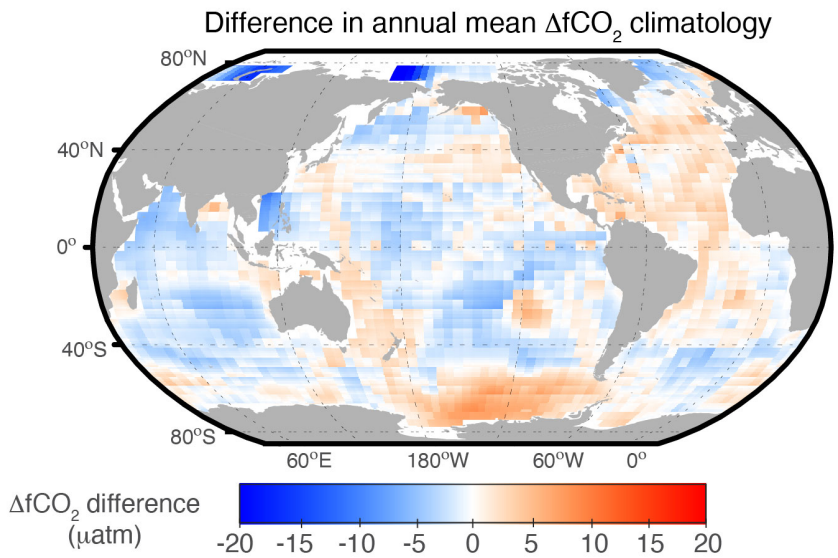

Supplementary Figure 6: Annual mean difference in ΔfCO_2 calculated from the SOCAT database using a constant 1.5μatm yr^{-1} time normalization minus the current ΔfCO_2 method.

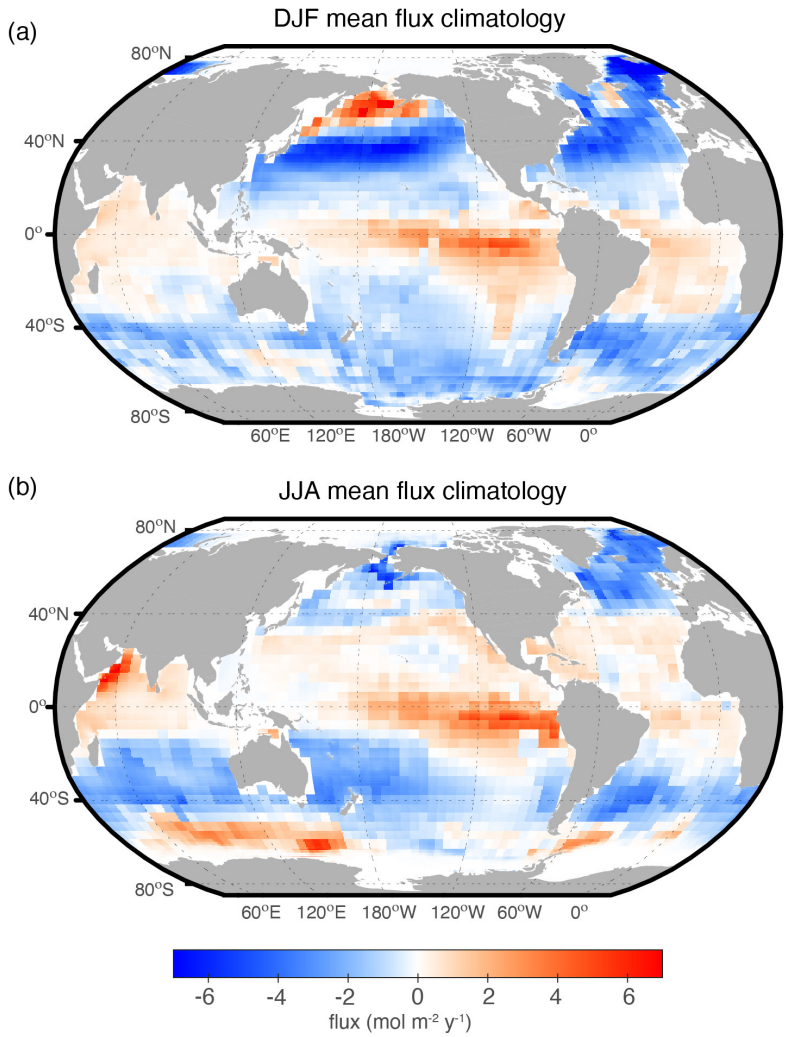

1705 Supplementary Figure 7: Seasonal sea–air CO_2 flux (mol C m^{-2} $year^{-1}$) climatology for (a) December, January, February (DJF) and (b) June, July, August (JJA) using the LDEO database. Positive values (warm colors) indicate sea-to-air fluxes (ocean efflux), and negative values (cool colors) indicate air-to-sea fluxes (ocean uptake).

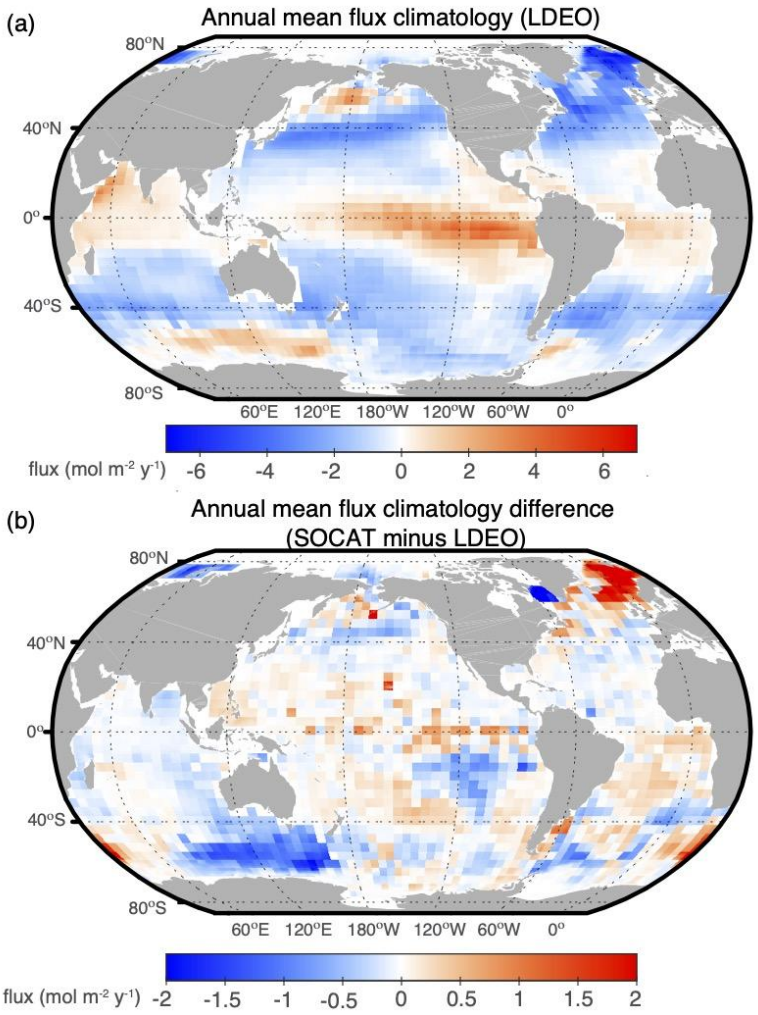

Supplementary Figure 8: (a) Annual mean CO_2 flux calculated from the LDEO database and (b) difference in flux between the SOCAT and LDEO database climatologies (SOCAT *minus* LDEO). Flux is calculated identically for each climatology, using the SeaFlux method using the mean of three wind speed reanalysis products. Warm colors indicate regions of carbon efflux and cool colors indicate regions of carbon uptake. The global mean flux is -1.79 PgC yr^{-1} for SOCAT and -1.68 PgC yr^{-1} for LDEO.

Deleted: ¶

¶

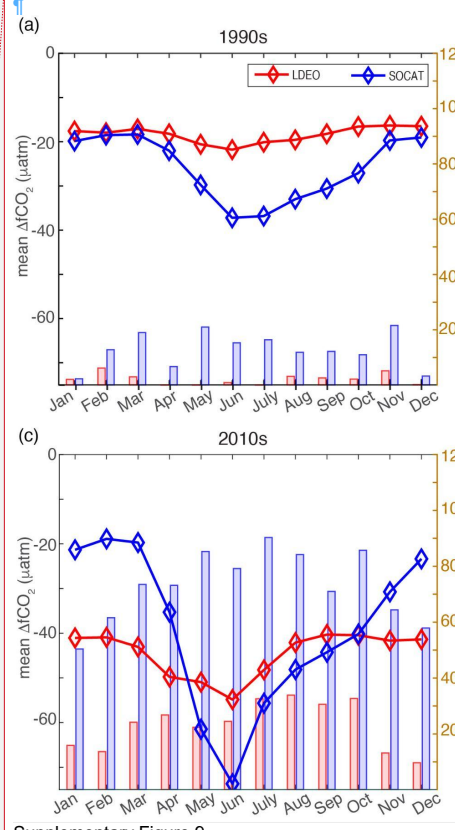

Supplementary Figure 9

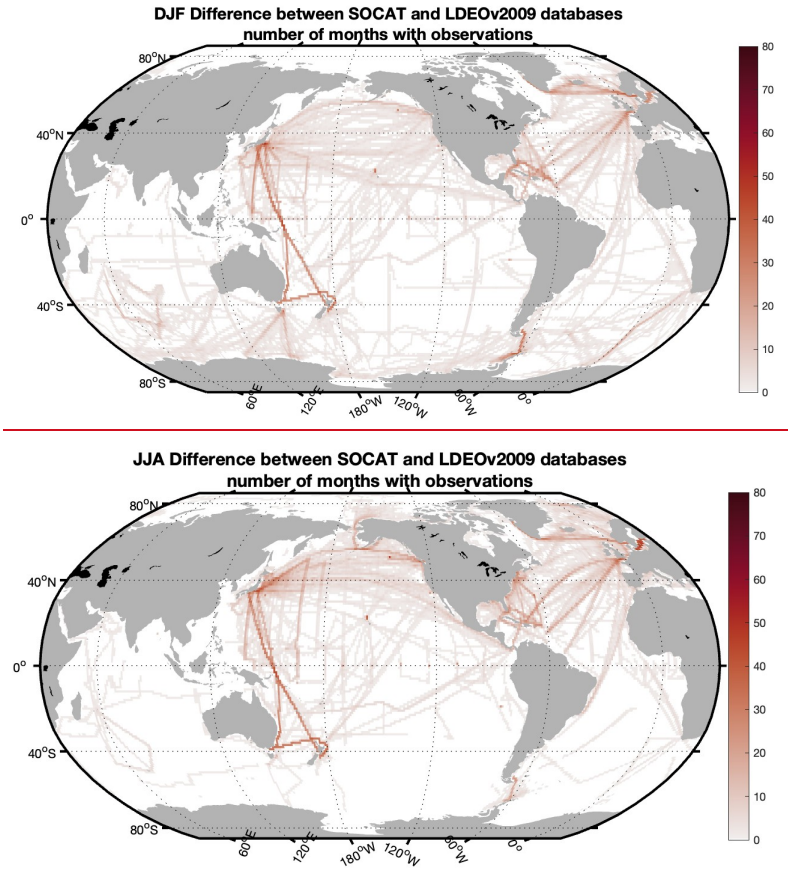

Supplementary Figure 9: Map showing number of additional months per gridcell for data in SOCATv2022 as compared to the LDEO dataset that was used in T-2009 for 2 seasons: December, January, and February (DJF) and June, July, and August (JJA). LDEOv2009 dataset includes observations through 2007 and SOCATv2022 includes observations through 2021.

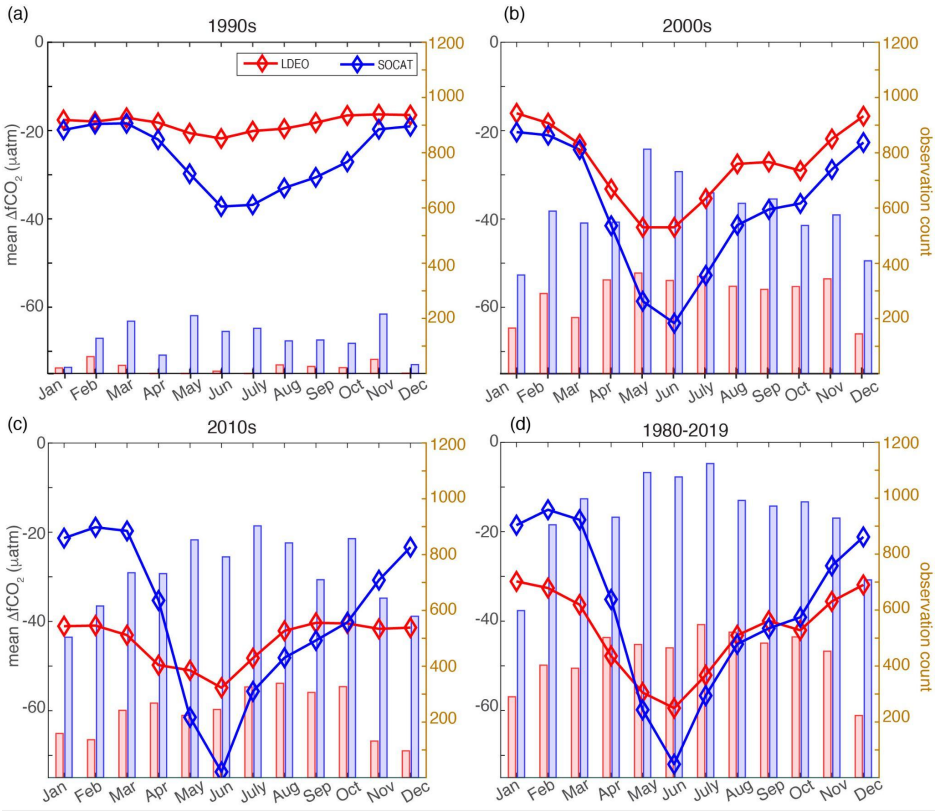

Supplementary Figure 10: Monthly mean values for sea-air ΔfCO_2 differences in the North Atlantic Subpolar biome. Average values for each month are plotted for the LDEO database (red) and the SOCAT database (blue) for each decade: (a) 1990-1999, (b) 2000-2009, (c) 2010-2019, and also the full common time period (1980-2019). Bar plots on each subplot show the number of 1ºx1º grid cells in this region which contain observations in the two databases.

Supplementary

Here we discuss the method and results based on observations included in the LDEOv2019 database to create an updated climatology. Comparisons are also made to the climatology discussed in the main text which is based on the SOCATv2022 database.

Methods

LDEO database

The LDEOv2019 database (available at https://www.ncei.noaa.gov/access/ ocean-carbon-acidification-data-system/oceans/LDEO_Underway_Database/, Takahashi et al. (2020)) consists of over 14 million measurements of pCO_2^{oce} with the earliest observations dating back to 1957 and the most recent collected in 2019 (Supplementary Figure 1). This database includes only pCO_2^{oce} values measured directly using the air–water equilibration method and requires that two or more standard gas mixtures were used for analyzer calibrations. This strict criteria for observation quality is unique to the LDEO database.

In this analysis, we restrict the time period to include observations collected beginning in 1980, which accounts for 99.9% of the available observations within the LDEOv2019 database. Additionally, we eliminate observations in the database that are not accompanied by both an observed sea surface temperature (SST) and atmospheric sea level pressure (SLP). Not only does this act to flag observations that might not be of the highest quality, it also allows a consistent methodology for creating the climatology from both the LDEO and SOCAT databases since the ancillary observations of SST and SLP are necessary to convert from pCO_2 to fCO_2, as well as to calculate a delta value, both steps which are essential in this updated climatology version.

Within the LDEO database, there are approximately 9400 observations without SST observations and nearly 755,000 missing SLP. Given instances where both SST and SLP are missing, the total number of omitted observations with this criteria is 764,115. Approximately 13.4 of the 14 million observations in the LDEO database meet all ancillary data requirements.

We have converted all pCO_2 observations in the LDEO database to fCO_2 values. As a pre-processing step, we have calculated fCO_2 values at the reported SST which helps to ensure a uniform representation of the surface ocean observations. The protocol for this conversion step follows that of the SOCAT methodology (Pfeil et al. 2013) which utilizes the equations recommended by Dickson et al. (2007) and requires observed temperature, salinity, and pressure.

Given the dramatic increase in pCO_2^{oce} measurements available since previous releases of the climatology (LDEOv2006, T-2009, and LDEOv2012, T-2014, included nearly 3 and 6.5 million observations, respectively, covering years 1970 to 2007 and 1957 to 2012, respectively), we do not remove the observations collected in the equatorial Pacific during El Niño years since inclusion does not strongly influence the overall result as in previous versions where those data made up a larger percentage of available observations.

There is a large overlap between the LDEO and SOCAT databases particularly for data prior to circa 2015. The LDEO and SOCAT databases are similar in that they restrict the included data to only observations that are measured in near-continuous operation or in discrete samples with an equilibrator system. Neither database includes pCO_2/fCO_2 measurements that are calculated from dissolved inorganic carbon, total alkalinity and/or pH.

Atmospheric fCO_2 calculation for LDEO database

For the LDEO database, the corresponding atmospheric CO_2 value is not included in the reported database as it is in the SOCAT database, so atmospheric CO_2 values from the NOAA MBL product (Lan et al. 2023) are matched based on month and location (latitude) of the pCO_2^{oce} observation. In calculating fCO_2 from pCO_2, we use the reported SLP, SST and salinity from the LDEO database.

Results

LDEO ΔfCO_2 climatology

Global

Supplementary Figure 2 shows the near-global annual climatological mean distribution of ΔfCO_2 (fCO_2^{oce} minus fCO_2^{air}) for both databases. Large-scale patterns across the global ocean incluce the consistent high (positive) ΔfCO_2 values in the equatorial Pacific where upwelling is a dominant influence, and low (negative) values of ΔfCO_2 in the North Atlantic physical processes including evaporation (increase salinity) and cooling drive strong uptake of carbon and subduction of surface waters.

As for SOCAT, the near-global LDEO ΔfCO_2 climatology curve has a bimodal shape (Supplementary Figure 3) with a smaller peak in boreal spring (March/April) and a larger peak in late boreal summer (August/September). The LDEO curve reaches its minimum in January and begins a recovery throughout the boreal winter before dipping again for a springtime minimum in May. While the overall pattern is similar between the SOCAT and LDEO curves, the LDEO curve has a larger amplitude, reaching a higher peak and lower trough. The near-global LDEO annual mean ΔfCO_2 value is -3.9 µatm.

Regional

The equatorial regions of the Pacific and Atlantic oceans have positive ΔfCO_2 values throughout the annual cycle and little seasonal variability (Supplementary Figure 3, 4ab). This indicates that these areas are sources of CO_2 to the atmosphere year round. The equatorial Pacific has the highest positive ΔfCO_2 values (annual mean of 31.5 µatm), followed by the tropical Atlantic (annual mean of 11.6 µatm, Supplementary Figure 4).

The subtropical biomes, representing the temperate North and South Atlantic and Pacific basins exhibit large seasonal ΔfCO_2 cycles which change sign throughout the year (Supplementary Figure 4); positive ΔfCO_2 occurs in warm summer months and negative values in colder winter months reflecting the dominance of seasonal temperature changes on the cycles of ΔfCO_2 in these regions. In the LDEO database, the seasonal amplitude for the subtropical North Pacific is 43.3 µatm, and is slightly larger than the seasonal amplitude in the subtropical North Atlantic (39.6 µatm). The same pattern is observed in the SOCAT database however with slightly larger amplitudes for both basins (Figure 4, Supplementary Figure 4). Since the mean seasonal amplitudes for SST are quite similar in these two oceans, with the Atlantic having a slightly larger seasonal change in surface temperature (4.4ºC in Pacific and 5.0ºC in Atlantic), the difference in ΔfCO_2 amplitudes between the Pacific and Atlantic subtropical regions cannot be attributed solely to SST, and may reflect differences in biogeochemical cycling between these two basins.

Seasonal changes in the northern subtropical oceans are roughly six months out of phase from the southern subtropical biomes. The South Pacific subtropical biome has significantly smaller seasonal amplitude than the corresponding Northern Hemisphere region; the South Pacific subtropical biome amplitude is 15.3 µatm. The amplitude in the South Atlantic subtropical basin is much more comparable to the North Atlantic (South Atlantic subtropical amplitude is 37.1 µatm). The Indian Ocean subtropical biome, which encompasses most of the Indian Ocean, both above and below the Equator, has a smaller amplitude (19.8 µatm) but the phasing matches well with the South Pacific and Atlantic biomes, with peak (positive) ΔfCO_2 values in February and the lowest values in August (Supplementary Figure 4). The low fCO_2 in the Indian and South Pacific subtropical basin is partially attributable to lower SST variability in these regions (SST seasonal cycle amplitudes are 4.0ºC in South Pacific and 3.0ºC in the Indian as compared to 4.6ºC in the South Atlantic) however it is likely that differences in spatiotemporal patterns of primary productivity also contribute to this difference. The striking difference in the amplitude of the cycle in the South Pacific and Indian subtropics could also be influenced by undersampling in these basins and in the Southern Hemisphere oceans overall.

The timing of the peak drawdown in the subpolar regions is opposite that observed in the subtropical North Pacific and Atlantic basins. A strong negative ΔfCO_2 in the spring to summer months is due to the effects of biological drawdown which quickly and dramatically lowers the CO_2 levels of the surface ocean. With its biological dependence and strongly stratified mixed layers, the subpolar region seasonal cycle are roughly four to six months out of phase with those from the adjacent subtropical regions. In the Atlantic subpolar biome, ΔfCO_2 values are consistently below zero throughout the annual cycle (maximum of -31.1 µatm occurs in January). In the Pacific basin, the ocean exceeds the atmospheric levels of fCO_2 in the boreal winter (Jan-March) before the spring bloom results in biological drawdown which lowers the ΔfCO_2 values below zero for the remainder of the year. The spring drawdown is weaker in the Pacific basin than the Atlantic.

Supplementary Figure 4c displays the seasonal cycle for the Southern Ocean biomes including the seasonal ice biome, the subpolar region, and the seasonally stratified subtropical region of the Southern Hemisphere. Unlike the subtropical regions of the other basins, this region has a relatively small seasonal ΔfCO_2 amplitude and has consistently negative ΔfCO_2 values (atmosphere>ocean) throughout the annual cycle. The mean of this Southern Ocean subtropical region is -20.9 µatm with a maximum amplitude of 9.1 µatm.

Unlike the seasonally-stratified subtropical region of the Southern Ocean, the Southern Ocean subpolar and ice biomes both have relatively strong seasonal cycles, reaching a maximum ΔfCO_2 of zero or slightly positive during the late austral winter and early austral spring (Supplementary Figure 4).

LDEO flux

The mean annual air-sea CO_2 flux for the LDEO database is -1.68 PgC yr^{-1} with negative indicating an uptake by the ocean. This represents a slightly greater flux into the ocean than the direct estimate from the previous version of the climatology (Takahashi et al. 2009) which estimated global mean flux at 1.4 PgC yr^{-1}. For the uncertainty in global ocean-atmosphere CO_2 flux reported here we use the value reported by Wanninkhof et al. (2013) as described above.

The global mean flux estimate presented here is for the area of the global ocean covered by this database and does not fully extend over the entire global ocean; it covers 90% of the global ocean. Specifically, coastal and high latitude regions are missing also as described above for the SOCAT database.

Supplementary Figure 7 shows the climatological seasonal mean sea–air CO_2 flux (mol m^{-2} yr^{-1}) for two seasons (DJF and JJA). The equatorial Pacific is the most prominent atmospheric CO_2 source region, with a seasonally persistent sea-to-air flux. When combined with the equatorial Atlantic region, the tropical belt emits an annual mean 0.35 PgC yr^{-1} to the atmosphere.

Adjacent to this tropical efflux zone lies an area of seasonally variable uptake patterns. The subtropical basins in both hemispheres act as CO_2 sinks in the cooler months and transition to regions of neutral or small CO_2 sources during the warmer months. At higher subtropical latitudes, strong winds and relatively low ocean fCO_2 occur along the subtropical convergence zone- a region where the cooled subtropical gyre waters with low fCO_2 meet the subpolar waters with biologically-lowered fCO_2.

The Northern Hemisphere subtropical region represents a smaller sink (-0.64 PgC yr^{-1}) than the corresponding Southern Hemisphere region (-0.82 PgC yr^{-1}), largely due to the overall greater size of the oceans in the Southern Hemisphere at these latitudes as noted above. There is also significant uptake in the Southern Ocean subtropical region (-0.55 PgC yr^{-1}).

Comparison of climatologies built from SOCAT and LDEO databases

Global

On a global scale, the monthly mean ΔfCO_2 seasonal amplitudes for the climatology produced using the LDEO database is larger than for the SOCAT database, reaching both higher in the boreal summer and lower in the boreal winter months. The LDEO climatology has an amplitude of 6.6 µatm while the SOCAT global mean climatology amplitude is 5.0 µatm (Supplementary Figure 2).

The mean annual air-sea CO_2 flux resulting from the LDEO version of the climatology created is -1.67 PgC yr^{-1}, with negative value indicating an uptake by the ocean. This represents a slightly greater flux into the ocean than the direct estimate from the previous version of the climatology (T-2009) which estimated global mean flux of -1.4 PgC yr^{-1}. This shift towards greater carbon uptake is consistent with other work indicating increased ocean uptake in recent decades (Friedlingstein et al. 2022, DeVries et al. 2023).

The LDEO climatology annual mean flux is slightly less negative than the mean global air-sea CO_2 flux based on the SOCAT database (-1.79 PgC yr^{-1}). While the overall shape of the seasonal cycle is comparable between the two databases, the amplitude in flux is much larger for the LDEO database, a result of the larger ΔfCO_2 global mean amplitude (Supplementary Figure 2). Specifically, the LDEO database has global mean flux values approaching zero during the boreal summer months, leading to a reduced uptake of carbon during these months. While the boreal winter months have similar flux estimates between the two databases, the difference during the months of July, August, and September ultimately reduce the overall global mean flux value reported from the LDEO database.

Southern Ocean

While the total annual Southern Ocean (<35S) flux estimates are similar (-1.04 PgC yr^{-1} and -0.90 PgC yr^{-1} for SOCAT and LDEO respectively), discrete regions of the Southern Ocean exhibit some of the largest differences in the climatological air-sea flux created from the SOCAT versus LDEO database (Figure 5, Supplementary Figure 6). Specifically, in the ocean region south of Australia, the SOCAT database produces flux estimates of larger carbon uptake/less efflux than the LDEO database. This signal of

larger uptake estimates in the SOCAT database is consistent throughout all months of the year but peaks during August, September, and October. These differences are likely a result of more available observations in the SOCAT database in this region (Figure 1, Supplementary Figure 1). Throughout the vast expanse of the remainder of the Southern Hemisphere subtropical and subpolar regions (i.e. the Pacific and Atlantic sectors), the differences are much smaller and heterogeneous (Figure 5, Supplementary Figure 6). Therefore, we do not see substantial biome-scale differences in the climatology of either ΔfCO_2 or carbon flux despite the small anomalous region south of Australia.

North Atlantic Subpolar Differences

For most regions of the global ocean, the ΔfCO_2 climatological cycle is consistent between the SOCAT and LDEO datasets (Figure 4, Supplementary Figure 4). Differences in the absolute magnitude of the ΔfCO_2 values are also observed in the equatorial regions in both the Atlantic and Pacific basins where SOCAT has slightly larger ΔfCO_2 values, but the overall shape and amplitude of the seasonal cycle is consistent between the two databases. One exception to this is the North Atlantic subpolar region where the differences in seasonal climatology between the two datasets are large. The North Atlantic subpolar region has similar total annual ΔfCO_2 estimates (-37.45 µatm and -42.33 µatm for SOCAT and LDEO respectively) but the seasonal differences are profound (Supplementary Figure 10).

Deleted: 9

The seasonal amplitude in the North Atlantic subpolar biome is over two times as large for the SOCAT database compared to the LDEO database (28.3 µatm in LDEO and 56.9 µatm in SOCAT; Figure 4 and Supplementary Figure 4). While the phasing and shape of the seasonal cycle is consistent between the two databases in this region, there is a significant difference in the amplitude of the winter to summer transition. While the winter (DJF) mean ΔfCO_2 is about 10 µatm different between the two (LDEO being more negative than SOCAT), the opposite is true for the summer season with the SOCAT showing more positive values. The transition to spring and summer blooms, when ΔfCO_2 is greatly reduced allowing for more uptake by the surface ocean, is very different between the two databases with a March to June change of 54.7 µatm in the SOCAT database versus 23.1 µatm for LDEO. Spring/Summer (MAM/JJA) ΔfCO_2 values for the LDEO database are -46.7and -51.6 µatm, respectively, while for the SOCAT database corresponding values are -37.4 and -57.9 µatm, respectively (Figure 4, Supplementary Figures 4 and 9). While an annual mean value in this region may not show a significant difference between the two databases, the differences in seasonal cycle amplitude are likely driven by mechanisms that are more completely captured by the higher sampling density of the SOCAT database and missed in LDEO.

The amplitude of the seasonal cycle increases with time from the 1990s to the 2000s in both databases, however it is the 2010-2019 time period that shows the strongest differences between the climatology produced by each database (Supplementary Figure 10). For the most recent decade (2010-2019), the amplitude of ΔfCO_2 calculated from the LDEO database actually decreases from the previous decade (14.6 µatm) while the amplitude from the SOCAT database is larger than any previous decade, exceeding 50 µatm in absolute amplitude (SOCAT amplitude is 54.8 µatm; Supplementary Figure 10c). The LDEO database is likely lacking sufficient seasonal observations to fully capture the biological drawdown that characterizes this region.

Deleted: 9

Deleted: 9c

Specifically, this stark contrast is likely due to the abundance of observations in the higher latitudes of the North Atlantic subpolar region in the SOCAT database around Iceland and extending into the Norwegian Sea (Figure 1, Supplementary Figure 1). This result is due both to differences in spatial and temporal coverage. Many grid cells in the version created from the SOCAT database include full seasonal coverage (twelve unique months of observations over the full time period considered). This subpolar North Atlantic is a very dynamic region particularly over the spring/summer months with strong biological drawdown of CO_2 in strongly stratified shallow mixed layers. In order to accurately capture the seasonal evolution of ΔfCO_2, it is imperative to have observations from each season. To capture the evolution of the seasonal cycle in this region over long time intervals requires near continuous full seasonal coverage of observations highlighting the importance of expanded efforts to observe the high latitude oceans.

Supplementary References

Takahashi, Taro; Sutherland, Stewart C.; Kozyr, Alex (2020). Global Ocean Surface Water Partial Pressure of CO2 Database: Measurements Performed During 1957-2019 (LDEO Database Version 2019) (NCEI Accession 0160492). Version 9.9. NOAA National Centers for Environmental Information. Dataset. https://doi.org/10.3334/CDIAC/OTG.NDP088(V2015)

Page 30: [1] Deleted A.R. Fay and coauthors 3/12/24 12:12:00 PM

Page 30: [1] Deleted A.R. Fay and coauthors 3/12/24 12:12:00 PM

Page 30: [1] Deleted A.R. Fay and coauthors 3/12/24 12:12:00 PM

Page 30: [1] Deleted A.R. Fay and coauthors 3/12/24 12:12:00 PM

Page 30: [1] Deleted A.R. Fay and coauthors 3/12/24 12:12:00 PM

Page 30: [1] Deleted A.R. Fay and coauthors 3/12/24 12:12:00 PM

Page 30: [1] Deleted A.R. Fay and coauthors 3/12/24 12:12:00 PM

Page 30: [1] Deleted A.R. Fay and coauthors 3/12/24 12:12:00 PM

Page 30: [1] Deleted A.R. Fay and coauthors 3/12/24 12:12:00 PM

Page 30: [1] Deleted A.R. Fay and coauthors 3/12/24 12:12:00 PM

Page 30: [1] Deleted A.R. Fay and coauthors 3/12/24 12:12:00 PM

Page 30: [1] Deleted A.R. Fay and coauthors 3/12/24 12:12:00 PM

Page 30: [1] Deleted A.R. Fay and coauthors 3/12/24 12:12:00 PM

Page 30: [1] Deleted A.R. Fay and coauthors 3/12/24 12:12:00 PM

Page 30: [1] Deleted A.R. Fay and coauthors 3/12/24 12:12:00 PM

Page 30: [1] Deleted A.R. Fay and coauthors 3/12/24 12:12:00 PM

Page 30: [1] Deleted A.R. Fay and coauthors 3/12/24 12:12:00 PM

Page 30: [1] Deleted A.R. Fay and coauthors 3/12/24 12:12:00 PM

Page 30: [1] Deleted A.R. Fay and coauthors 3/12/24 12:12:00 PM

Page 30: [1] Deleted A.R. Fay and coauthors 3/12/24 12:12:00 PM

Page 30: [1] Deleted A.R. Fay and coauthors 3/12/24 12:12:00 PM

Page 30: [1] Deleted A.R. Fay and coauthors 3/12/24 12:12:00 PM

Page 30: [1] Deleted A.R. Fay and coauthors 3/12/24 12:12:00 PM

Page 30: [1] Deleted A.R. Fay and coauthors 3/12/24 12:12:00 PM

Page 30: [1] Deleted A.R. Fay and coauthors 3/12/24 12:12:00 PM

Page 30: [1] Deleted A.R. Fay and coauthors 3/12/24 12:12:00 PM

Page 30: [1] Deleted A.R. Fay and coauthors 3/12/24 12:12:00 PM

Page 30: [1] Deleted A.R. Fay and coauthors 3/12/24 12:12:00 PM

Page 30: [1] Deleted A.R. Fay and coauthors 3/12/24 12:12:00 PM

Page 30: [1] Deleted A.R. Fay and coauthors 3/12/24 12:12:00 PM

Page 30: [1] Deleted A.R. Fay and coauthors 3/12/24 12:12:00 PM

Page 30: [1] Deleted A.R. Fay and coauthors 3/12/24 12:12:00 PM

Page 30: [1] Deleted A.R. Fay and coauthors 3/12/24 12:12:00 PM

Page 30: [1] Deleted A.R. Fay and coauthors 3/12/24 12:12:00 PM

Page 30: [1] Deleted A.R. Fay and coauthors 3/12/24 12:12:00 PM

Page 30: [1] Deleted A.R. Fay and coauthors 3/12/24 12:12:00 PM

Page 30: [1] Deleted A.R. Fay and coauthors 3/12/24 12:12:00 PM

Page 30: [1] Deleted A.R. Fay and coauthors 3/12/24 12:12:00 PM

Page 30: [1] Deleted A.R. Fay and coauthors 3/12/24 12:12:00 PM

Page 30: [1] Deleted A.R. Fay and coauthors 3/12/24 12:12:00 PM

Page 30: [1] Deleted A.R. Fay and coauthors 3/12/24 12:12:00 PM

Page 30: [1] Deleted A.R. Fay and coauthors 3/12/24 12:12:00 PM

Page 30: [1] Deleted A.R. Fay and coauthors 3/12/24 12:12:00 PM

Page 30: [1] Deleted A.R. Fay and coauthors 3/12/24 12:12:00 PM

Page 30: [1] Deleted A.R. Fay and coauthors 3/12/24 12:12:00 PM

Page 30: [1] Deleted A.R. Fay and coauthors 3/12/24 12:12:00 PM

Page 30: [1] Deleted A.R. Fay and coauthors 3/12/24 12:12:00 PM

Page 30: [1] Deleted A.R. Fay and coauthors 3/12/24 12:12:00 PM

Page 30: [1] Deleted A.R. Fay and coauthors 3/12/24 12:12:00 PM

Page 30: [1] Deleted A.R. Fay and coauthors 3/12/24 12:12:00 PM

Page 30: [1] Deleted A.R. Fay and coauthors 3/12/24 12:12:00 PM

Page 30: [1] Deleted A.R. Fay and coauthors 3/12/24 12:12:00 PM

Page 30: [1] Deleted A.R. Fay and coauthors 3/12/24 12:12:00 PM

Page 30: [1] Deleted A.R. Fay and coauthors 3/12/24 12:12:00 PM

Page 30: [1] Deleted A.R. Fay and coauthors 3/12/24 12:12:00 PM

Page 30: [1] Deleted A.R. Fay and coauthors 3/12/24 12:12:00 PM

Page 30: [1] Deleted A.R. Fay and coauthors 3/12/24 12:12:00 PM

Page 30: [1] Deleted A.R. Fay and coauthors 3/12/24 12:12:00 PM

Page 30: [1] Deleted A.R. Fay and coauthors 3/12/24 12:12:00 PM

Page 30: [1] Deleted A.R. Fay and coauthors 3/12/24 12:12:00 PM

Page 30: [1] Deleted A.R. Fay and coauthors 3/12/24 12:12:00 PM

Page 30: [1] Deleted A.R. Fay and coauthors 3/12/24 12:12:00 PM

Page 30: [1] Deleted A.R. Fay and coauthors 3/12/24 12:12:00 PM

Page 30: [1] Deleted A.R. Fay and coauthors 3/12/24 12:12:00 PM

Page 30: [1] Deleted A.R. Fay and coauthors 3/12/24 12:12:00 PM

Page 30: [1] Deleted A.R. Fay and coauthors 3/12/24 12:12:00 PM

Page 30: [1] Deleted A.R. Fay and coauthors 3/12/24 12:12:00 PM

Page 30: [1] Deleted A.R. Fay and coauthors 3/12/24 12:12:00 PM

Page 30: [1] Deleted A.R. Fay and coauthors 3/12/24 12:12:00 PM

Page 30: [1] Deleted A.R. Fay and coauthors 3/12/24 12:12:00 PM

Page 30: [1] Deleted A.R. Fay and coauthors 3/12/24 12:12:00 PM

Page 30: [1] Deleted A.R. Fay and coauthors 3/12/24 12:12:00 PM

Page 30: [1] Deleted A.R. Fay and coauthors 3/12/24 12:12:00 PM

Page 30: [1] Deleted A.R. Fay and coauthors 3/12/24 12:12:00 PM

Page 30: [1] Deleted A.R. Fay and coauthors 3/12/24 12:12:00 PM

Page 30: [1] Deleted A.R. Fay and coauthors 3/12/24 12:12:00 PM

Page 30: [1] Deleted A.R. Fay and coauthors 3/12/24 12:12:00 PM

Page 30: [1] Deleted A.R. Fay and coauthors 3/12/24 12:12:00 PM

Page 30: [1] Deleted A.R. Fay and coauthors 3/12/24 12:12:00 PM

Page 30: [1] Deleted A.R. Fay and coauthors 3/12/24 12:12:00 PM

Page 30: [1] Deleted A.R. Fay and coauthors 3/12/24 12:12:00 PM

Page 30: [1] Deleted A.R. Fay and coauthors 3/12/24 12:12:00 PM

Page 30: [1] Deleted A.R. Fay and coauthors 3/12/24 12:12:00 PM

Page 30: [1] Deleted A.R. Fay and coauthors 3/12/24 12:12:00 PM

Page 30: [1] Deleted A.R. Fay and coauthors 3/12/24 12:12:00 PM

Page 30: [1] Deleted A.R. Fay and coauthors 3/12/24 12:12:00 PM

Page 30: [1] Deleted A.R. Fay and coauthors 3/12/24 12:12:00 PM

Page 30: [1] Deleted A.R. Fay and coauthors 3/12/24 12:12:00 PM

Page 30: [1] Deleted A.R. Fay and coauthors 3/12/24 12:12:00 PM

Page 30: [1] Deleted A.R. Fay and coauthors 3/12/24 12:12:00 PM

Page 30: [1] Deleted A.R. Fay and coauthors 3/12/24 12:12:00 PM

Page 30: [1] Deleted A.R. Fay and coauthors 3/12/24 12:12:00 PM

Page 30: [1] Deleted A.R. Fay and coauthors 3/12/24 12:12:00 PM

Page 30: [1] Deleted A.R. Fay and coauthors 3/12/24 12:12:00 PM

Page 30: [1] Deleted A.R. Fay and coauthors 3/12/24 12:12:00 PM

Page 30: [1] Deleted A.R. Fay and coauthors 3/12/24 12:12:00 PM

Page 30: [1] Deleted A.R. Fay and coauthors 3/12/24 12:12:00 PM

Page 30: [1] Deleted A.R. Fay and coauthors 3/12/24 12:12:00 PM

Page 30: [1] Deleted A.R. Fay and coauthors 3/12/24 12:12:00 PM

Page 30: [1] Deleted A.R. Fay and coauthors 3/12/24 12:12:00 PM

Page 30: [1] Deleted A.R. Fay and coauthors 3/12/24 12:12:00 PM